NASA Contractor Report 165706

INVESTIGATION OF AERODYNAMIC CHARACTERISTICS OF WINGS HAVING VORTEX FLOW USING DIFFERENT NUMERICAL CODES

C. Subba Reddy

OLD DOMINION UNIVERSITY RESEARCH FOUNDATION
Norfolk, Virginia 23508

Grant NSG-1561
April 1981

National Aeronautics and Space Administration

Langley Research Center
Hampton, Virginia 23665

INVESTIGATION OF AERODYNAMIC CHARACTERISTICS OF WINGS HAVING VORTEX FLOW USING DIFFERENT NUMERICAL CODES

SUMMARY

The aerodynamic characteristics of highly sweptback wings having separation-induced vortex flows have been investigated by employing different numerical codes with a view to determining some of the capabilities and limitations of these codes. Flat wings of various configurations—strake wing models, cropped, diamond, arrow and double delta wings, have been studied. Cambered and cranked planforms have also been tested.

The theoretical results predicted by the codes have been compared with the experimental data, wherever possible, and found to agree favorably for most of the configurations investigated. However, highly cambered wings could not be successfully modeled by the codes. It appears that the final solution in the free vortex sheet method is affected by the selection of the initial solution. Accumulated span loadings estimated for delta and diamond wings have been found to be unusual in comparison with attached flow results in that the slopes of these load curves near the leading edge do not tend to infinity as they do in the case of attached flow.

INTRODUCTION

This report briefly describes the work performed under grant NSG 1561 during the period from September 1, 1978 to August 31, 1979. In this work six- and nine-parameter versions of the free vortex sheet (FVS) method of the Boeing Company (refs. 1 and 2), quasi-vortex lattice (QVL) method of Mehrotra (refs. 3 and 4), and vortex lattice method with suction analogy (VLM-SA) of Langley Research Center (refs. 5 to 7) have been employed to study various configurations with a view to determining the code capabilities and limitations. More emphasis has been given to

testing the nine-parameter version of the FVS method than the others as the latter were already tested (ref. 8). This version employs two types of solution procedures: iterative and least squares schemes. The former scheme has been commonly used to model almost all the wings and the latter, which is expensive to execute, to model only the wings for which the former failed to provide converged results. The iterative scheme cannot handle wings with streamwise edges or highly cambered wings. However, it can successfully model wings with streamwise edges provided these edges and the sharp bends on the leading edges are replaced by smooth curves.

The models studied include flat and cambered wings of different configurations. The details of these configurations are given in tables 1 to 3. The results are discussed here, and some of the numerical code capabilities and limitations are brought into focus.

NOMENCLATURE

a	notch height
a/ℓ	notch ratio
A	aspect ratio
APC	parameter that determines the initial location of vortex sheet in the FVS method
b	wing span
$b(x)$	local wing span
c	local wing chord
$\bar{c}$	mean aerodynamic chord
c_{ℓ_a}	accumulated sectional life coefficient
c_r	wing root chord
C_L	lift coefficient
C_{L_D}	design lift coefficient

C_m	pitching moment coefficient, about 0.25 $\bar{c}$
FVS	free vortex sheet (6- or 9-parameter version)
FVS(6-PV)	free vortex sheet (6-parameter version)
FVS(9-PV)	free vortex sheet (9-parameter version)
ℓ	distance between apex and tip along x-axis
M	Mach number
QVL	quasi-vortex lattice
VLM-SA	vortex lattice method with suction analogy
x,y,z	body axis coordinates
α	angle of attack
δ_t	tip rake angle
θ	angle through which tip edge moved with respect to original position
ΔC_D	drag due-to-lift coefficient
ΔC_p	difference between upper and lower surface pressure coefficients

RESULTS

In this section, the results obtained by employing the three numerical codes are compared with the existing data wherever possible and some of the code capabilities and limitations are discussed.

A summary of the various wing configurations investigated using different computer codes is presented in tables 1 to 3. The range of angle of attack and aspect ratio over which the codes are employed and whether or not the solutions given by the FVS and QVL methods are converged are also indicated in the tables. The results obtained by the FVS method correspond to no near-wake modeling unless otherwise stated.

Flat wings

Strake wing models (ref. 9).— Figures 1 to 5 show the comparison of data with the results obtained by the FVS method for a series of double delta wings (models 1 to 5). These are the strake wing models, the basic configuration (model 1) of which has an 80° inboard sweep, 65° outboard sweep, pointed tip, and an unswept trailing edge. The other models include cropped double-delta (model 2), cropped double-arrow (model 3), cropped delta (model 4), and double-arrow (model 5). The agreement between the theoretical lift and drag coefficients and the data is good for models 1, 2, and 4 (figs. 1, 2, and 4), especially at lower angles of attack, and it is fairly good for the wings with sweptback trailing edges (models 3 and 5, figs. 3 and 5). The predicted pitching moment and the data do not compare well in general. With a view to improving the performance of the code, near-wake modeling has also been adopted in certain cases with some success. This aspect is discussed in greater detail later under the heading "Discussion."

Cropped wings (ref. 10).— The theoretical and experimental longitudinal aerodynamic characteristics for a family of cropped wings are presented in figures 6 to 8. These wings are sharp-edged configurations (cropped diamond, delta, and arrow wings with constant leading edge), with constant tip chord, sweep angle of 63° and trailing-edge sweep angles of -40°, 0°, and 40°, respectively. The agreement between the predicted C_L, C_D, and C_m values and the data is very good (figs. 6 and 7) in the tested angle-of-attack range of 15° to 25° for the cropped delta and cropped diamond wings. But the method is unable to provide adequate results for the cropped arrow, as indicated in the figure 8, especially in the case of pitching moment. This limitation of the code, namely the inability to successfully model the arrow wings, is also seen in the case of the models 3 and 5 (ref. 9), which also have the sweptback trailing edges. However, much better results have been obtained, as illustrated in figure 8, when the wing was slightly modified by replacing the streamwise edge by a smooth curve. This aspect is further discussed in detail in the next section, titled "Discussion."

Asymmetrical cropped delta wing (ref. 11).— This wing has a sweep angle of 63° and rake angle varying from -3° to 13°. In order to facilitate solution convergence for this wing, the right-hand side with its sharp bend and streamwise edge has been replaced by a smooth curve. More details on this type of approximation are given later in this report in the "Discussion" section. Figure 9 shows the effect of rake angle on the lift characteristics of an asymmetrical delta wing. The lift here is based on the reference area corresponding to the planform with $\delta_t = 0$. The predicted lift shows the same trend as the data, and the agreement between them is fairly good.

Delta and diamond wings (ref. 12).— Figures 10 and 16 show the accumulated span loadings for 70° delta and diamond wings. These loadings are estimated from the results obtained by the FVS(6-PV) method, and following the same procedure described in reference 8. These are unusual in comparison with the attached flow results. The slopes of the curves near the leading edge do not go to infinity as they do in the case of attached flow. However, it should be noted here that the above curves have been obtained from the integration of ΔCp's at a limited number of locations on the wing.

Cambered Wings

Nangia's wings (ref. 13).— The theoretical lift coefficients obtained by the FVS(6-PV), QVL, and VLM-SA methods for A = 1 spanwise cambered delta (wing B) are compared with the data in figure 17. The agreement between the theory and experiment is reasonable. The predicted pitching moments by the codes are also shown in the same figure; there is no agreement between the codes. The corresponding data for the pitching moment is not available to make a direct comparison.

Figure 18 shows the spanwise pressure distribution at two locations for the same wing. The theoretical pressures given by the FVS(6-PV) and QVL methods and the data do not agree well. However, the former provides better results than the latter. It gives a pressure peak, but slightly outboard of the wing compared to the data.

The lift and pitching moment coefficients for Nangia's wing C, which has a large chordwise camber (9.46%), are shown in figure 19. The FVS(6-PV) method fails to give converged results. The other methods yield results which do not agree well with the data. However, the VLM-SA method gives better overall agreement with the C_L data even though it has a peculiar behavior around $C_L = 1.0$. This may be associated with the reattachment of the leading edge vortex changing sides mostly from lower to upper wing surface.

Squire's wings (ref. 14).— Figures 20 to 23 show the aerodynamic characteristics of spanwise cambered wings (wings 4 to 7). Some of the results have already been reported in reference 8; however, for the sake of completeness, those results are also reproduced in these figures. Here the theoretical values are compared with the experimental values of Squire (ref. 14); the agreement is generally good. The FVS(9-PV) is unable to model wings 6 and 7, which have larger cambers, except at higher angles of attack for wing 6. The results predicted by the QVL method for wing 7 are also not in good agreement with the data.

Wentz's apex cambered wing (ref. 15). — The longitudinal aerodynamic characteristics obtained by the QVL method are compared with Wentz's data in figure 24. The agreement between them is fairly good except in the case of pitching moment. Figures 25 to 27 depict the spanwise pressure distributions for the same wing at different angles of attack. As can be seen from the figures, the agreement between the predicted values and the data is not good.

75° cambered delta wing (ref. 16).— This wing has an attached-flow-design $C_{L_D} = 0.3$. Figure 28 compares the longitudinal aerodynamic characteristics of the wing obtained by the three numerical methods. The FVS(9-PV) and the QVL methods agree well with each other, up to $\alpha = 23°$, whereas the VLM-SA predicts higher C_L and lower ΔC_D than the other two. The spanwise pressure distribution obtained by the FVS(9-PV) and QVL methods at various chordwise locations are compared in figures 29 to 33. There is no good agreement between the two results. However, it is expected that the results of the FVS(9-PV) method may be closer to reality because they show well-defined pressure peaks which indeed exist in an actual flow. As

there is no experimental data available, only the theoretical results are compared here.

71.6° cambered arrow wing.— The theoretical results obtained by the QVL method are compared with the experimental values (wind-tunnel test data obtained at NASA/Langley Research Center) in figure 34. The agreement is fair. The FVS method has failed to give a converged solution for this wing.

DISCUSSION

The discussion of the results presented in the preceding section has brought into focus some of the capabilities and limitations of the numerical codes. In this section they are discussed in greater detail.

Figure 35 shows the cropped delta wing (ref. 10) and the modified wing with the streamwise edge and the sharp bend on the leading edge replaced by a smooth curve. The wing has been modified, keeping the area of the wing almost the same, to eliminate the streamwise edge and thereby facilitate the application of the iterative scheme of the FVS(9-PV) method to model the wing. The unmodified and modified wings have been modeled using least squares and iterative schemes of the FVS(9-PV) method respectively, and the results are shown in table 4. Both the results are essentially the same and they compare well with the data. However, the computational time requirement for the least squares scheme is much more (about two times) than that for the iterative scheme. Therefore, it appears it is advisable to model such wings with streamwise edges by the iterative scheme after modifying the edge as indicated above.

The wing has been modified in another way as shown in figure 36 by varying the position of the tip edge with respect to the original position. An investigation has been carried out by systematically varying the tip-edge position ($0° \leq \theta \leq 5°$) to determine the minimum value of θ for which the iterative scheme of the method could give converged results. For this investigated range of θ, there has been no convergence. If θ is increased further, the solution may converge. But this has not been done because doing so might alter the wing considerably.

The main difference in the modifications made in figures 35 and 36 is only the sharp bend on the leading edge. It seems such a sharp bend has hindered the solution.

The effects of the near-wake modeling on the aerodynamic results for a double arrow wing have been studied, and these results are compared with the data in table 5. In one case, the near-wake has been confined to the notch portion of the wing, and in another it has been extended to a length equal to a root-chord length. It appears, from the results, that the length of the near-wake does not have much influence on the final solution. However, the near-wake does improve the accuracy of the results.

Several attempts have been made, with different starting solutions, to model a 75° highly cambered wing (ref. 17) by the FVS(9-PV) method, and some converged solutions have been obtained. These results are shown in table 6, and the final free-sheet shapes and positions are illustrated in figure 37. It is found that two converged but different solutions are obtained by the method for the same problem with different starting free-sheet positions. Therefore, it appears the solution is not unique, and the correct one should be determined using engineering judgment.

No converged solution has been obtained by the FVS(9-PV) method for McDonnell Douglas AST wing (ref. 18), even after the planform has been modified and simplified. This wing has a moderate aspect ratio and a large camber.

Table 7 shows the comparison of the aerodynamic results obtained by the 6- and 9-parameter versions of the FVS method and the data for A = 1.46 planar delta wing (ref. 12). The 9-parameter version has not provided any better overall results than the 6-parameter version. Increasing the number of panels also has not improved the accuracy.

The QVL method cannot generally model high aspect ratio wings. However, it can handle such wings provided the angle of attack is high. For example, it could not handle an aspect ratio 4 wing (ref. 19) at $\alpha = 10.36°$ or 20°, but it could handle the same wing at $\alpha = 40°$.

CONCLUSIONS

Flat and cambered wings of different configurations have been investigated using mainly the nine-parameter version of the free vortex sheet [FVS(9-PV)] and the quasi-vortex lattice (QVL) methods. Cropped wings, which could not be handled by the six-parameter version of the free vortex sheet [FVS(6-PV)] and QVL methods, have been studied by the FVS(9-PV) method. The vortex lattice method with suction analogy (VLM-SA) which will produce results for these wings has rarely been utilized herein. The details are as follows:

The least squares scheme of the FVS(9-PV) method has been used to study the wings with streamwise edges as the iterative scheme cannot handle such wings without modifying the geometry. The results obtained are in fairly good agreement with the experimental data. However, the least squares scheme is expensive compared to the other, and gives results which do not agree well with the data for the wings with swept-back trailing edges. It has severe limitations on the number of panels in free and fed sheets.

The iterative scheme of the FVS(9-PV) method has been applied to wings with streamwise edges after these edges and the sharp corners on the leading edges are replaced by smooth curves. Good results have been obtained by this approach at much less computer cost. Therefore, it appears this approach is preferable to the least squares scheme in such cases. The effect of near-field wake on the solution by this method has been studied and found to provide some improvement in the results. The lift coefficients obtained by this method for an asymmetrical wing with various rake angles compare fairly well with the data.

The FVS(6-PV) method, the QVL method, and the VLM-SA method have been employed to study Nangia's chordwise cambered wings B and C. All methods have handled wing B, and only the latter two handled wing C, which has larger camber, but the agreement between the data and the theoretical results is not satisfactory. The FVS(9-PV) method, though an improved version, could not successfully model large cambered wings, whereas the QVL method could model some of them. It appears that the selection of the initial solution affects the final solution in the case of the FVS

(9-PV) method, and this, of course, is undesirable in any method. Therefore, the correct answer has to be determined using engineering judgment in such cases where the initial solution plays a crucial role.

The QVL method has been used to investigate Wentz's apex cambered delta and Squire's spanwise cambered wings 4 to 7. The results are in good agreement with the data. This method can also handle high aspect ratio wings provided the angle of attack is high. For example, it could not handle an aspect ratio 4 wing at an angle of attack of 10.36° or 20°, but could handle the same wing at an angle of attack of 40°.

Also, accumulated span loadings have been determined for a delta and a diamond wing. These span loadings are unusual in comparison with attached flow results in that the slopes of the curves near the leading edge do not tend to infinity as they do in the case of attached flow.

REFERENCES

1. Brune, G.W.; Weber, J.A.; Johnson, F.T.; Lu, P.; and Rubbert, P.E.: A Three-Dimensional Solution of Flows over Wings with Leading-Edge Vortex Separation. Part I. Engineering Document, NASA CR-132709, 1975.

2. Johnson, F.T.; Lu, P.; Tinoco, E.N.; and Epton, M.A.: An Improved Panel Method for the Solution of Three-Dimensional Leading-Edge Vortex Flows. Volume 1 Theory Document. NASA CR-3278, 1980.

3. Mehrotra, S.C.: A theoretical Investigation of the Aerodynamics of Low Aspect-Ratio Wings with Partial Leading-Edge Separation. NASA CR-145304, 1978.

4. Mehrotra, S.C.; and Lan, C.E.: A Computer Program for Calculating Aerodynamic Characteristics of Low-Aspect Ratio Wings with Partial Leading-Edge Separation. NASA CR-145362, 1978.

5. Polhamus, E.C.: A Concept of the Vortex Lift of Sharp-Edge Delta Wings Based on a Leading-Edge Suction Analogy. NASA TN D-3767, 1966.

6. Margason, R.J.; and Lamar, J.E.: Vortex-Lattice Fortran Program for Estimating Subsonic Aerodynamic Characteristics of Complex Planiforms. NASA TN D-6142, 1971.

7. Lamar, J.E.; and Gloss, B.B.: Subsonic Aerodynamic Characteristics of Interacting Lifting Surfaces with Separated Flow Around Sharp Edges Predicted by a Vortex-Lattice Method. NASA TN D-7921, 1975.

8. Reddy, C.S.: Theoretical Study of Aerodynamic Characteristics of Wings Having Vortex Flow. NASA CR-159184, 1979.

9. Lamar, J.E.: Analysis and Design of Strake-Wing Configurations. J. Aircraft, Vol. 17, No. 1, 1980, pp. 20-27.

10. Lamar, J.E.: Extension of Leading-Edge-Suction Analogy to Wings with Separated Flow Around the Side Edges at Subsonic Speeds. NASA TR R-428, 1974.

11. Lamar, J.E.: Some Recent Applications of the Suction Analogy to Vortex Lift Estimates. NASA TM X-72785.

12. Wentz, W.H.; Jr.; and Kohlman, D.L.: Wind-Tunnel Investigation of Vortex Breakdown on Slender Sharp-Edged Wings. NASA CR-98737, 1968.

13. Nangia, R.K.: The Effects of Longitudinal Camber on Slender Wings. Ph.D. Dissertation, Univ. of London, 1967.

14. Squire, L.C.: Camber Effects on the Nonlinear Lift of Slender Wings with Sharp Leading Edges. Aeronautical Research Council C.P. No. 924, Ministry of Technology (London), 1967.

15. Wentz, W.H.: Effects of Leading-Edge Camber on Low Speed Characteristics of Slender Delta Wings. NASA CR-2002, 1972.

16. Lamar, J.E.: A Vortex-Lattice Method for the Mean Camber Shapes of Trimmed Nonplanar Planforms with Minimum Vortex Drag. NASA TN D-8090, 1976.

17. Lamar, J.E.: Subsonic Vortex-Flow Design Study for Slender Wings. J. Aircraft, Vol. 15, No. 9, pp. 611-617, 1978.

18. Radkey, R.L.; Wedge, H.R.; and Felix, J.E.: Aerodynamic Characteristics of a Mach 2.2 Advanced Supersonic Cruise Aircraft Configuration at Mach Numbers from 0.5 to 2.4. NASA CR-145094, 1977.

19. Lamar, J.E.: Longitudinal Aerodynamic Characteristics of 45° Swept Wings at Mach ≈ 0. NASA TM X-73942, 1976.

20. Tinoco, E.N.; Lu, P.; and Johnson, F.T.: An Improved Panel Method for the Solution of the Three-Dimensional Leading-Edge Vortex Flows. Volume II. Users Guide and Programmers Guide. NASA CR-3279, 1980.

Table 1. Wing configurations modeled by the FVS method. All cases have been modeled by the FVS(9-PV) method unless otherwise stated.

Number	Wing Description	Angle of Attack	Mach Number	Solution Converged?
	FLAT WINGS			
A1	80°/65° double delta, A = 160 [model 1 (ref. 9)]	15°-30°	0	yes
A2	80°/65° cropped double delta, A = 0.95 [model 2 (ref. 9)]	15°-30°	0	yes
A3	80°/65° cropped double arrow, A = 1.1 [model 3 (ref. 9)] (Note: Converges only after the straight tip is replaced by a curve)	15°-30°	0	yes
A4	80° cropped delta, A = 0.27 [model 4 (ref. 9)]	15°-35°	0	yes
A5	80°/65° double arrow, A = 2.08 [model 5 (ref. 9)]	15°-25°	0	yes
A6	63° cropped delta, A = 0.87 (ref. 10)	15°-25°	0.2	yes
A7	63° cropped diamond, A = 0.74 (ref. 10)	15°-25°	0.2	yes
A8	63° cropped arrow, A = 1.07 (ref. 10) (Note: Converges for α = 20° if the straight tip and sharp corner on the leading edge are replaced by a curve)	15°-25°	0.2	no
A9	63° asymmetrical cropped delta, basic planform A = 0.87 δ_t = -3° to 13° (ref. 11)	23°	0	yes
A10[a]	70° delta, A = 1.46 (ref. 12)	15°-40°	0	yes
A11[a]	70° diamond, A = 1.0 (ref. 12)	15°-40°	0	yes

(cont'd)

Table 1. (Concluded).

Number	Wing Description	Angle of Attack	Mach Number	Solution Converged?
	CAMBERED WINGS			
A12(a)[a]	76° delta, A = 1 [Nangia's wing-B (ref. 13)]	10°	0	no
A12(b)[a]	76° delta, A = 1 [Nangia's wing-B (ref. 13)]	23.8°,30°	0	yes
A13	76° delta, A = 1 [Nangia's wing-C (ref. 13)]	20°	0	no
A14[a]	76° delta, A = 1 [Squire's wing-4 (ref. 14)]	15°-40°	0	yes
A15(a)	76° delta, A = 1 [Squire's wing-5 (ref. 14)]	10°	0	no
A15(b)	76° delta, A = 1 [Squire's wing-5 (ref. 14)]	20°,30°	0	yes
A16(a)	76° delta, A = 1 [Squire's wing-6 (ref. 14)]	10°	0	no
A16(b)	76° delta, A = 1 [Squire's wing-6 (ref. 14)]	20°,30°	0	yes
A17	76° delta, A = 1 [Squire's wing-7 (ref. 14)]	20°	0	no
A18	75° delta, A = 1.07, attached flow C_{L_D} = 0.3 (ref. 16)	2°-30°	0	yes
A19	75° delta, A = 1.07, separated flow C_{L_D} = 0.3 (ref. 17)	-8°-10°	0	—[b]
A20	71.6° cropped arrow, A = 1.38	20°	0	no
A21	71°/57° cropped double arrow, A = 1.84 (ref. 18)	20°	0	no

[a]Case has been modeled using the FVS(6-PV) method

[b]In some cases, solution has converged to different values for the same α but with different initial free sheet shapes.

Table 2. Wing configurations modeled by the QVL method.

Number	Wing Description	Angle of Attack	Mach Number	Solution Converged?
B1(a)	45° flat delta, A = 4 (ref. 19)	10.36°,20°	0	no
B1(b)	45° flat delta, A = 4 (ref. 19)	40°	0	yes
B2	76° chordwise cambered delta [Nangia's wing-B (ref. 13)]	10°-30°	0	yes
B3	76° chordwise cambered delta [Nangia's wing-C (ref. 13)]	10°,30°	0	yes
B4	76° spanwise cambered delta [Squire's wings-4 to 7 (ref. 14)]	15°-30°	0	yes
B5	74° apex cambered delta wing, A = 1.15 (ref. 15)	10°-40°	0	yes
B6	75° cambered delta, A = 1.07, attached flow C_{L_D} = 0.3 (ref. 16)	-4°-30°	0	yes[a]
B7	75° cambered delta, A = 1.07 separated flow C_{L_D} = 0.3 (ref. 17)	-2°-2°	0	yes[a]
B8	71.6° cambered arrow[b] A = 1.38	0°-30°	0.6	yes[a]

[a]Though converged results are obtained for $\alpha < 6.3°$, the leading edge elements in the X-Z plane are flat and too close to the wing surface; hence the accuracy of the results is doubtful.

[b]This wing is actually cambered cropped arrow; but, since the code cannot handle cropped wings, it is approximated to an arrow wing.

Table 3. Wing configurations modeled by the VLM-SA.

Number	Wing Description	Angle of Attack	Mach Number
C1	76° chordwise cambered delta, A = 1 [Nangia's wings B and C (ref. 13)]	-10°-40°	0
C2	75° cambered delta, A = 1.07, attached flow C_{L_D} = 0.3 (ref. 16)	-10°-40°	0

Table 4. Comparison of aerodynamic characteristics of modified and original planar cropped delta wing (ref. 10); $\alpha = 20°$; $M \simeq 0$.

Wing description and the method used	C_L	ΔC_D	$-C_m$
Original wing; least squares scheme—FVS(9-PV) method	0.865	0.315	0.059
Modified wing; iterative scheme—FVS(9-PV) method	0.867	0.315	0.065
Original wing; data	0.874	0.325	0.060

Table 5. Effect of near-wake modeling on the solution of planar double-arrow wing (ref. 9); FVS(9-PV) method; $\alpha = 20°$; $M \simeq 0$.

Description	C_L	ΔC_D	$-C_m$
Extended near wake (extended to a length of 1 c_r)	0.771	0.281	0.134
Near wake confined to the notch portion	0.761	0.277	0.129
No near wake	0.972	0.354	0.267
Data	0.832	0.312	0.165

Table 6. Effect of starting solution on the final results for 75° cambered delta wing (ref. 17); free sheet rotated through 30°; FVS(9-PV) method; $\alpha = 10°$; $M = 0$.

APC (refs. 1,2,20)	C_L	ΔC_D	$-C_m$
0.25	0.360	0.085	0.056
0.50	0.540	0.106	0.107

Table 7. Comparison of 6- and 9-parameter versions of the FVS method; A = 1.46 planar delta wing (ref. 12) aerodynamic results; $\alpha = 25°$; M = 0.

Description	C_L	ΔC_D	$-C_m$
FVS(6-PV) method; number of panels = 30	1.115	0.520	0.151
FVS(9-PV) method; number of panels = 25; least squares scheme	1.202	0.560	0.207
FVS(9-PV) method; number of panels = 49; least squares scheme	1.243	0.580	0.185
Data	1.10	--	0.07

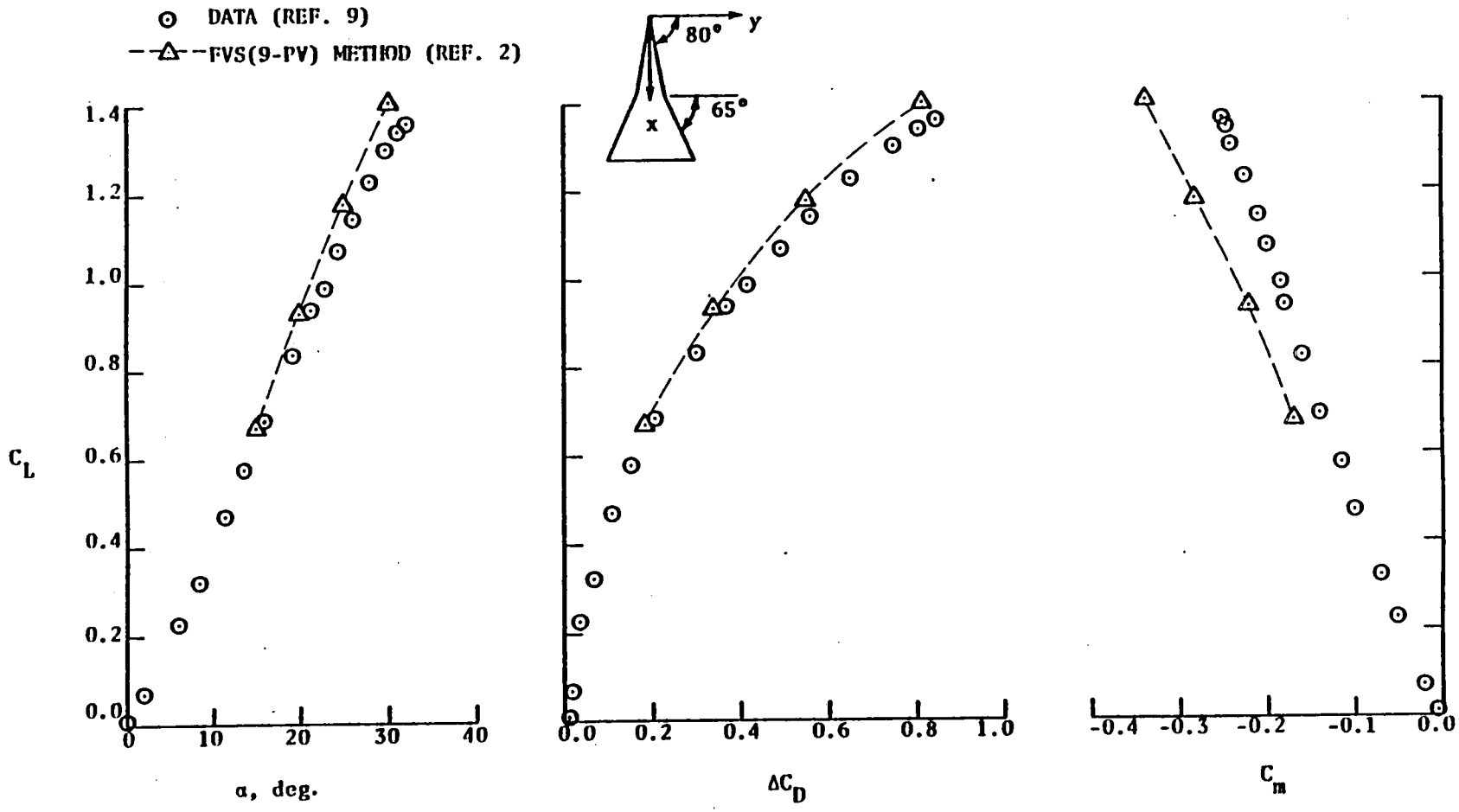

Figure 1. Longitudinal aerodynamic characteristics of A = 1.60 flat double delta wing (model 1); M ≈ 0.

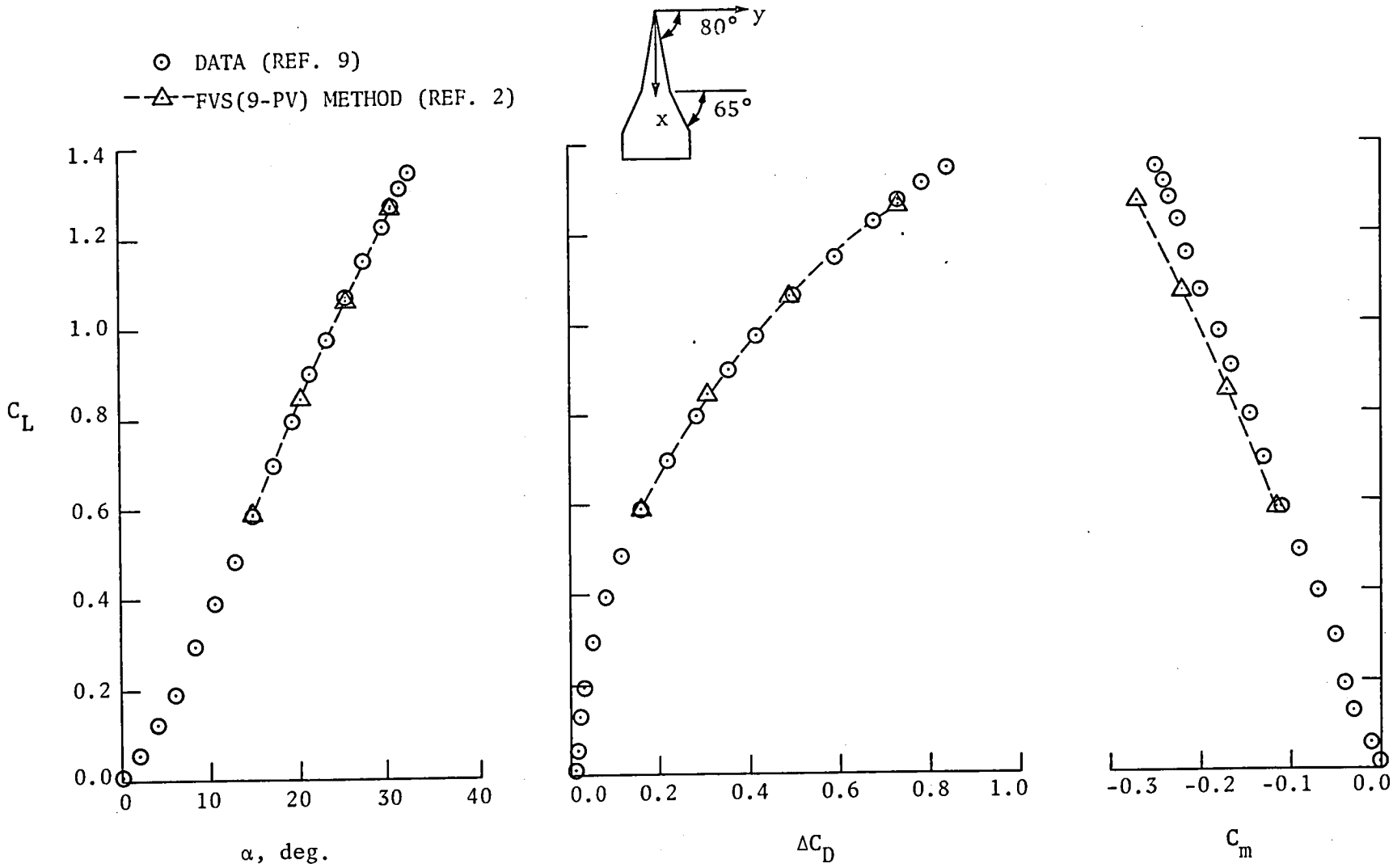

Figure 2. Longitudinal aerodynamic characteristics of A = 0.95 flat cropped double delta wing (model 2); M ≃ 0.

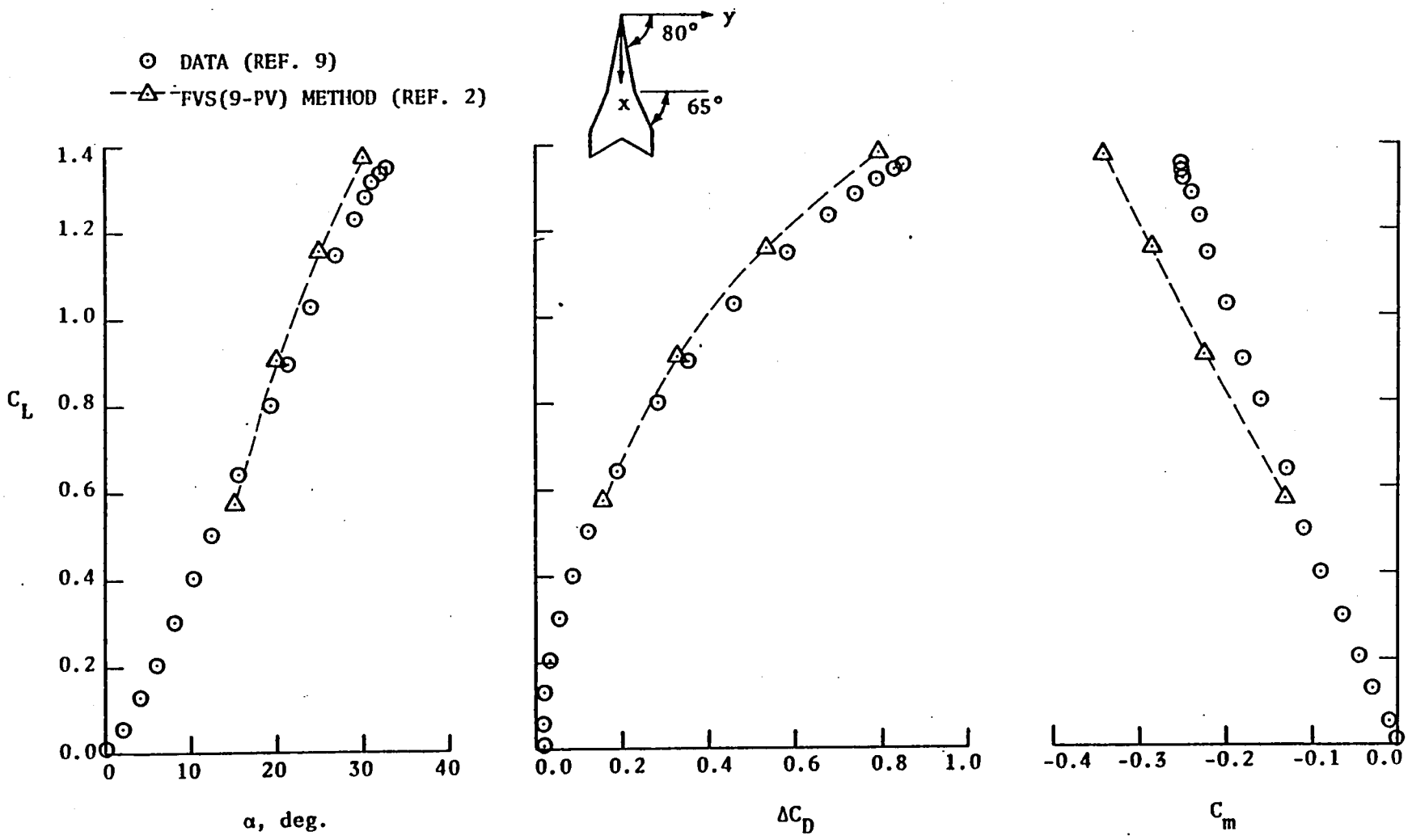

Figure 3. Longitudinal aerodynamic characteristics of A = 1.10 flat cropped arrow wing (model 3); M = 0.

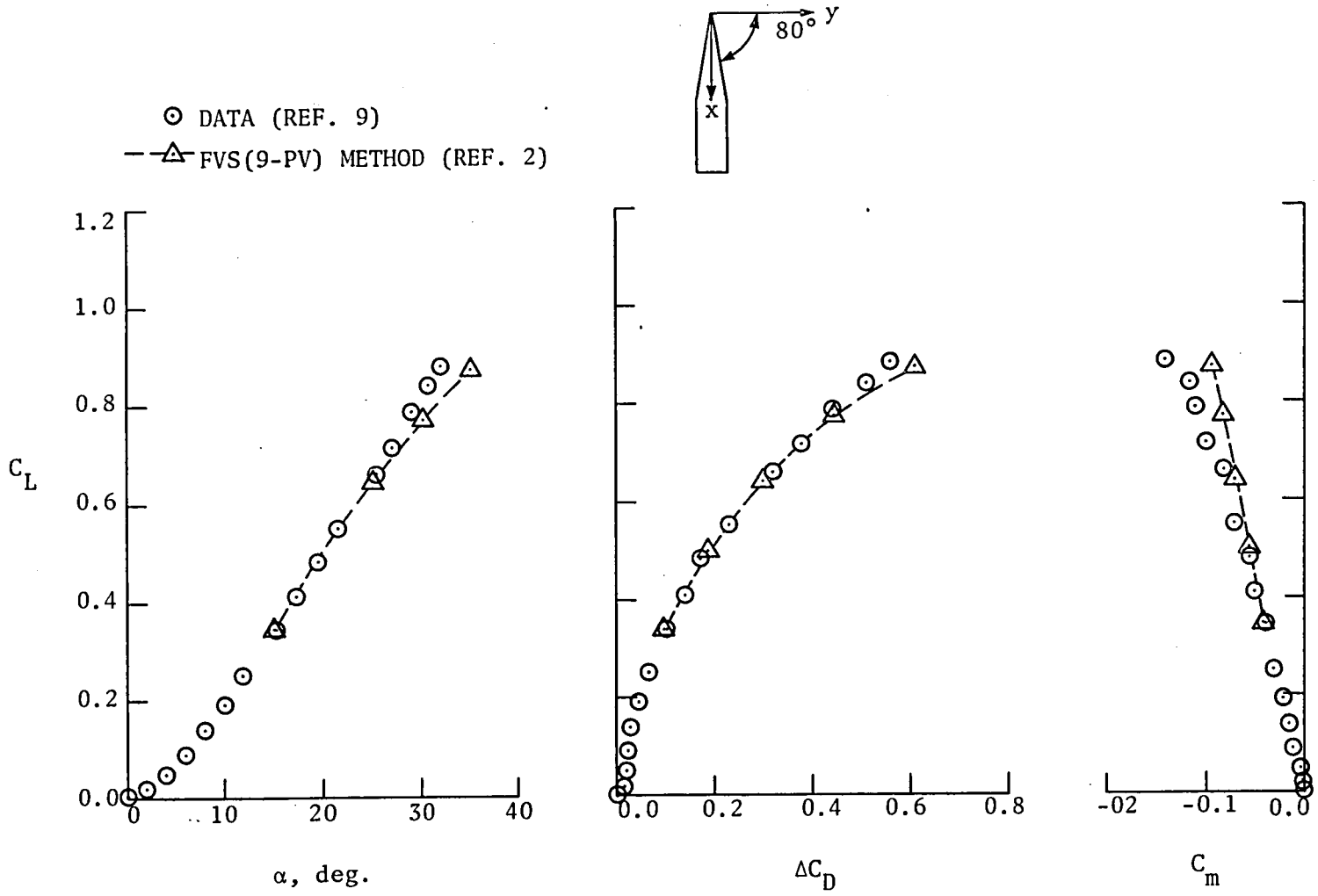

Figure 4. Longitudinal aerodynamic characteristics of A = 0.27 flat cropped delta wing (model 4); M ≈ 0.

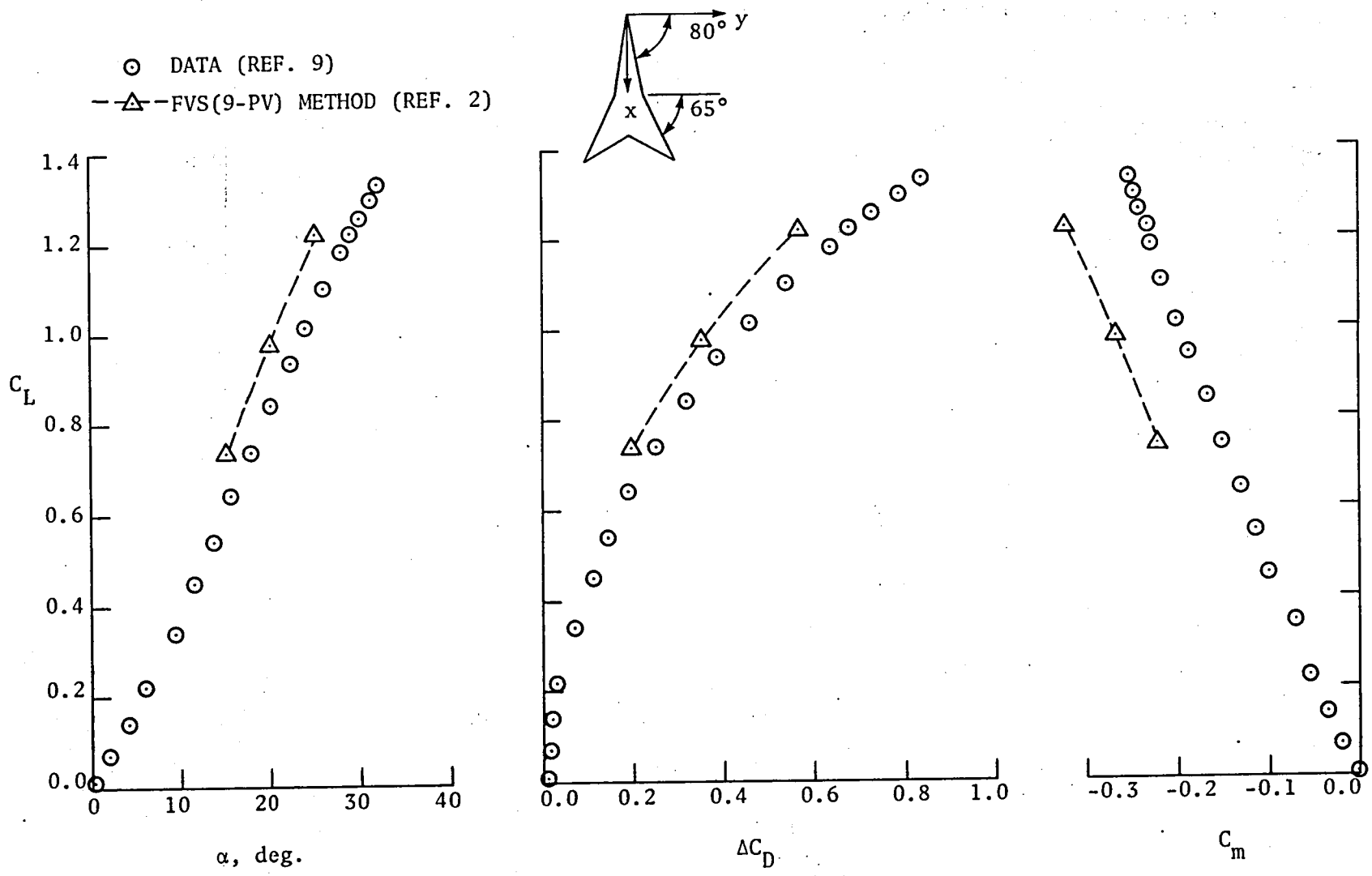

Figure 5. Longitudinal aerodynamic characteristics of A = 2.0 flat double arrow wing (model 5); M ≈ 0.

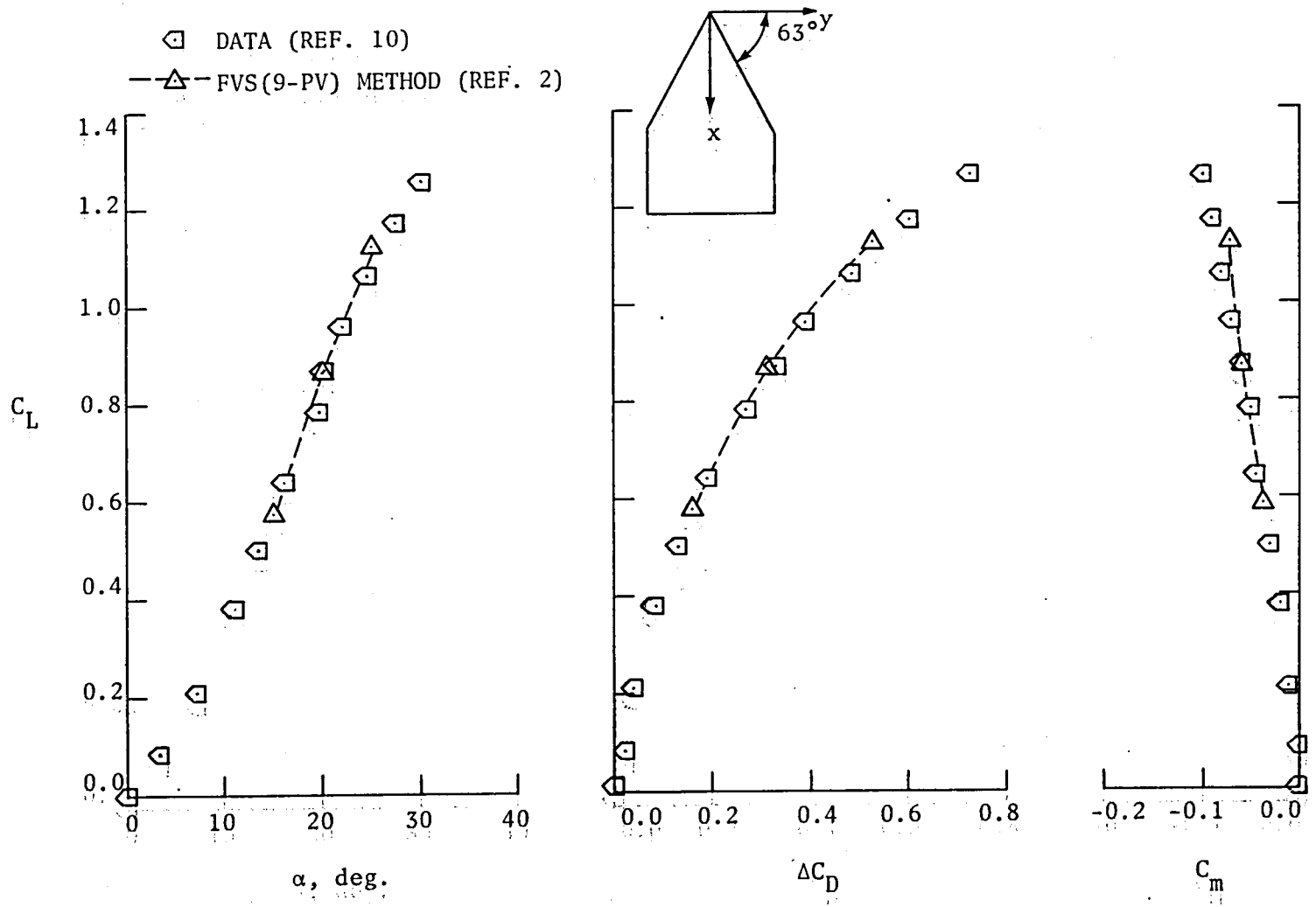

Figure 6. Longitudinal aerodynamic characteristics of A = 0.87 flat cropped delta wing; M = 0.2.

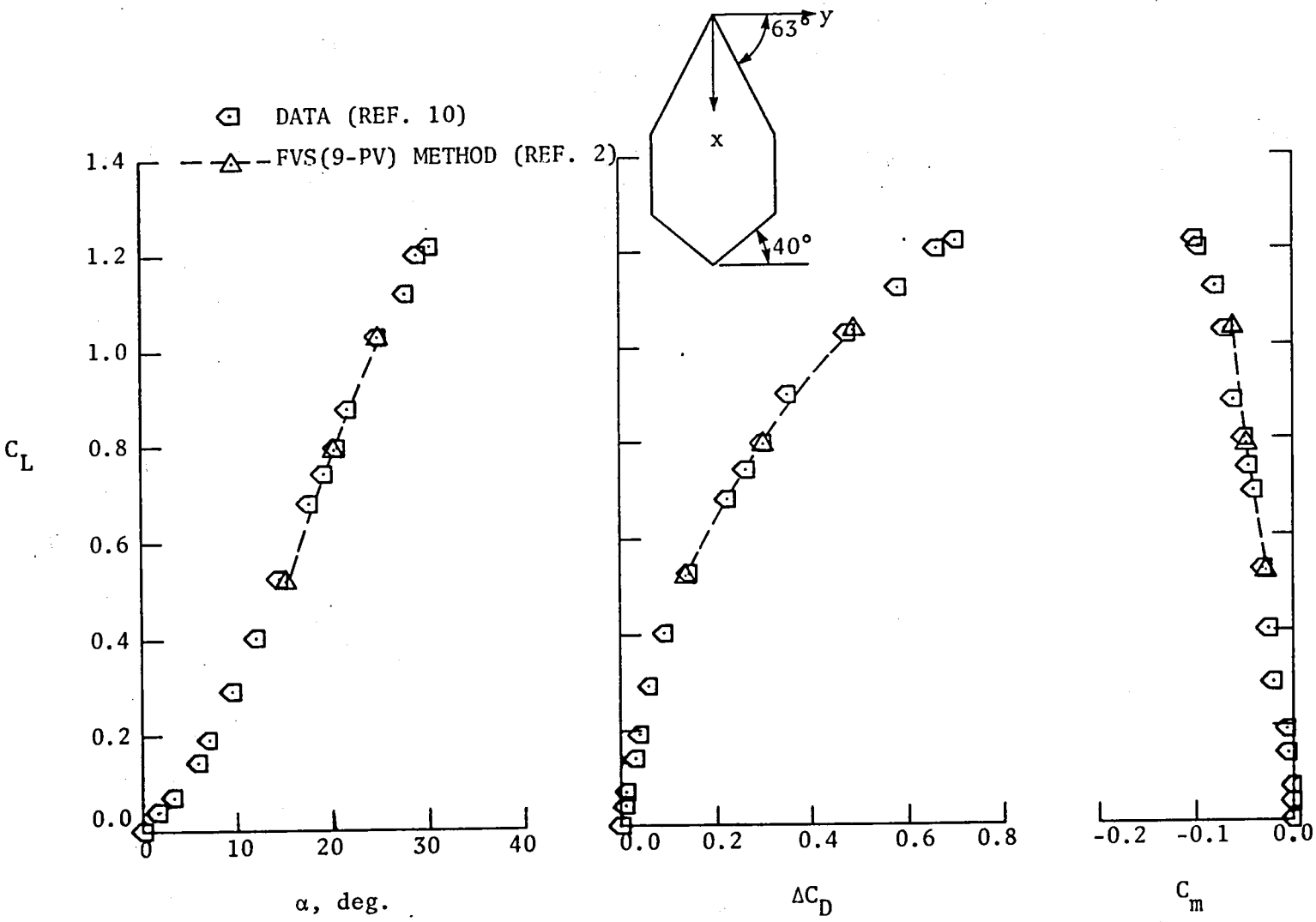

Figure 7. Longitudinal aerodynamic characteristics of A = 0.74 flat cropped diamond wing; M = 0.2.

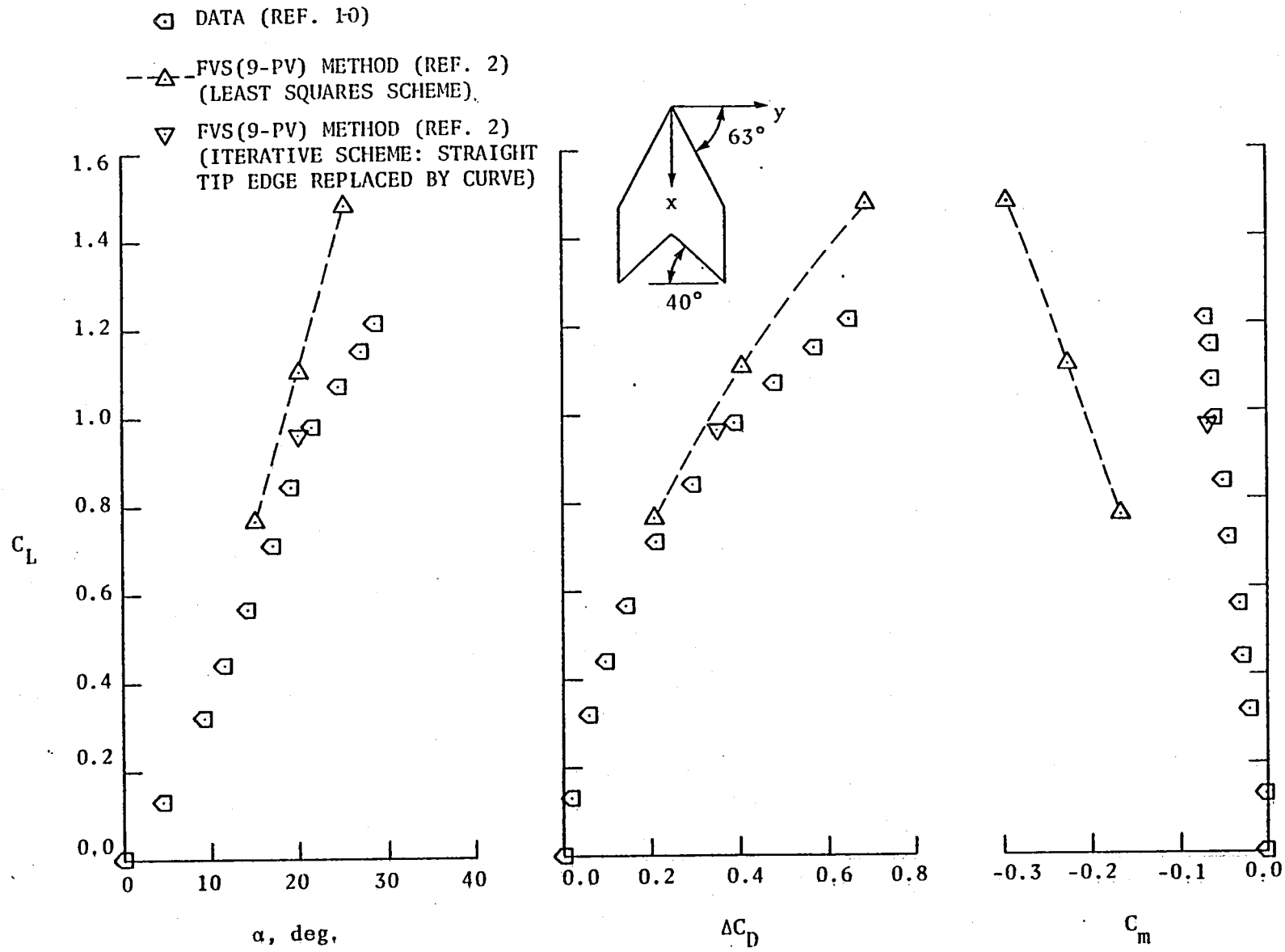

Figure 8. Longitudinal aerodynamic characteristics of A = 1.07 flat cropped arrow wing; M = 0.2.

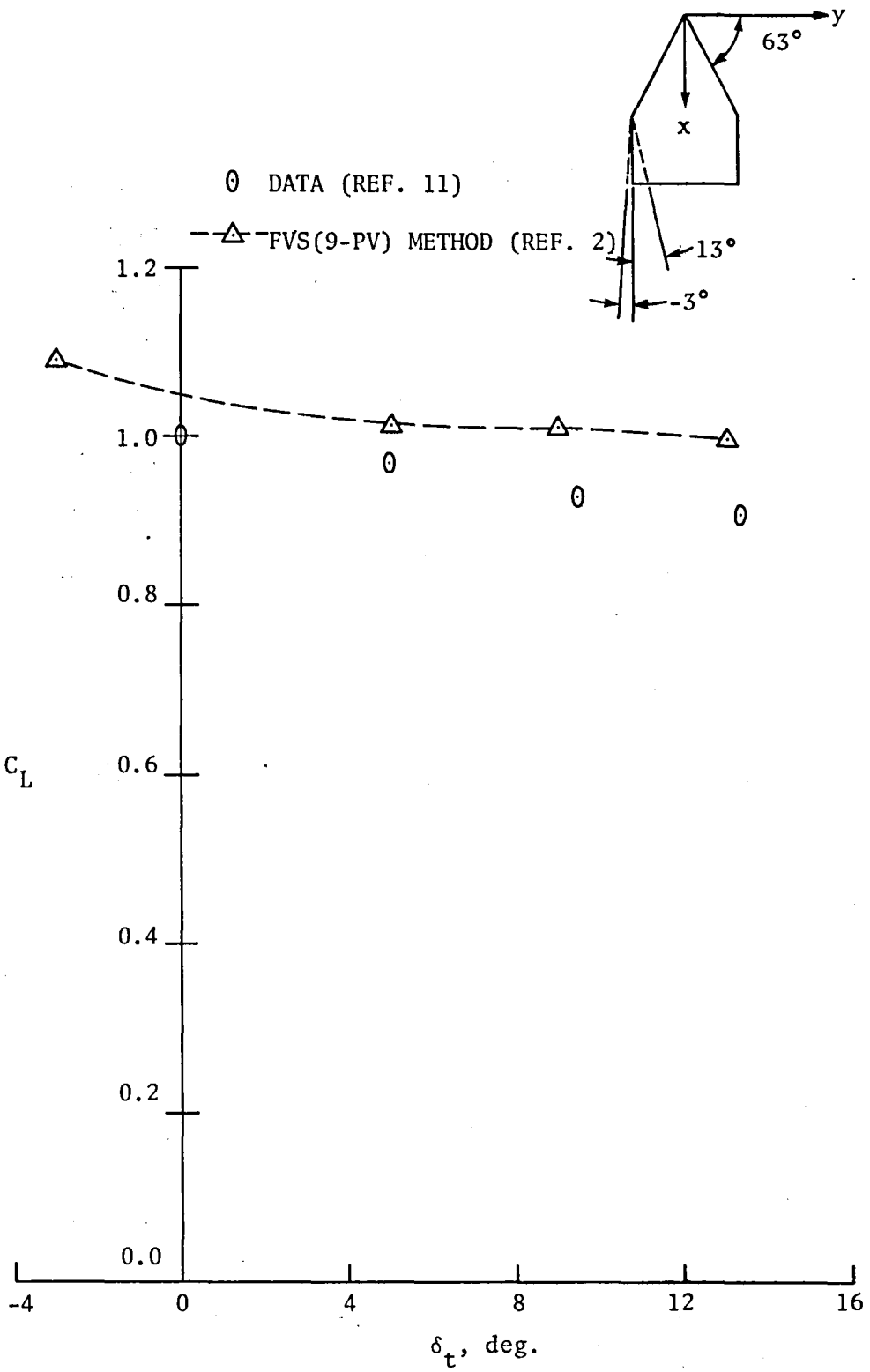

Figure 9. Effect of rake angle on lift coefficient for flat asymmetrical wing; $\alpha \approx 23°$; $M \approx 0$.

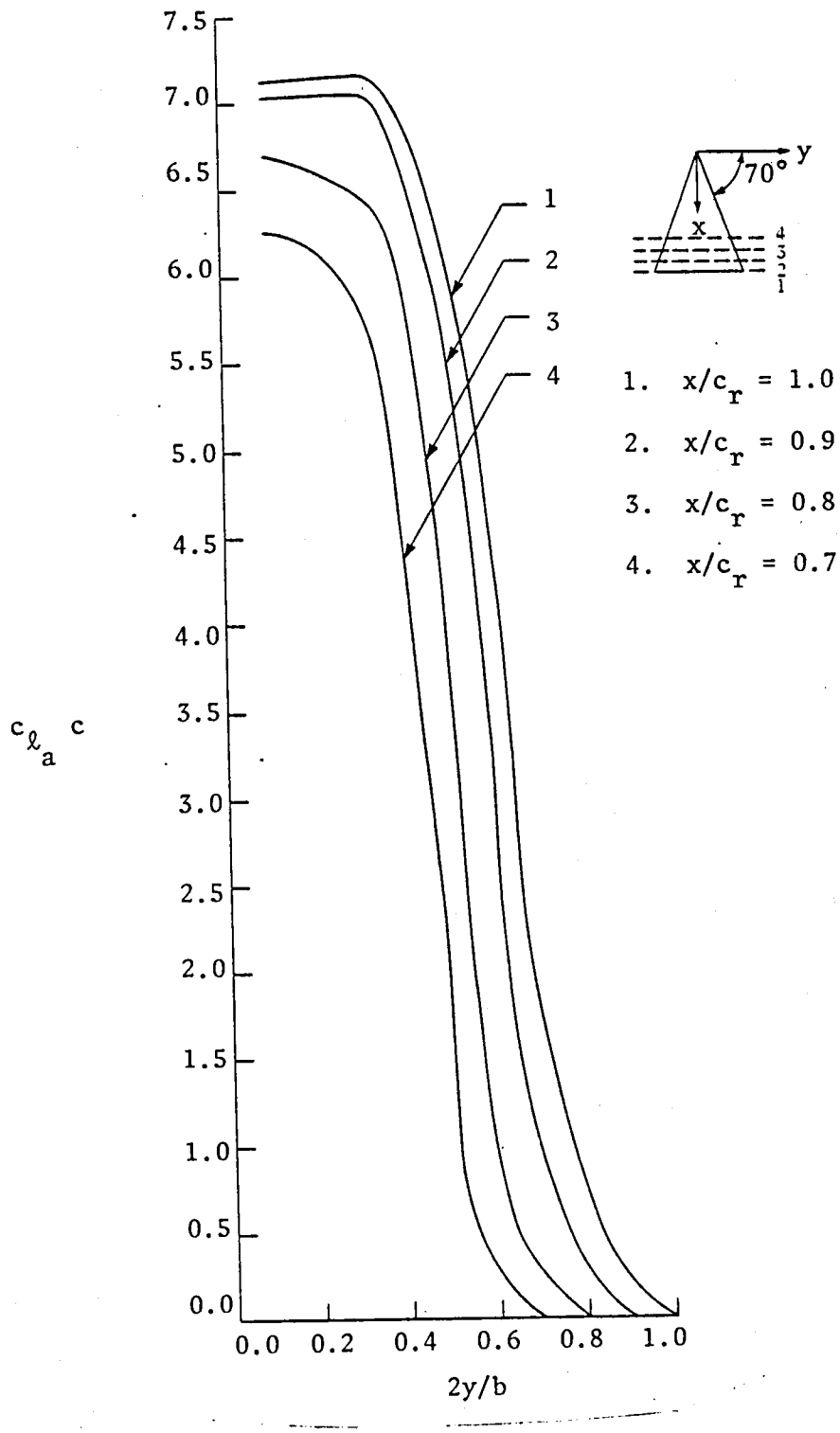

Figure 10. Accumulated span loadings for A = 1.46 flat delta wing at $\alpha = 15°$; M = 0.

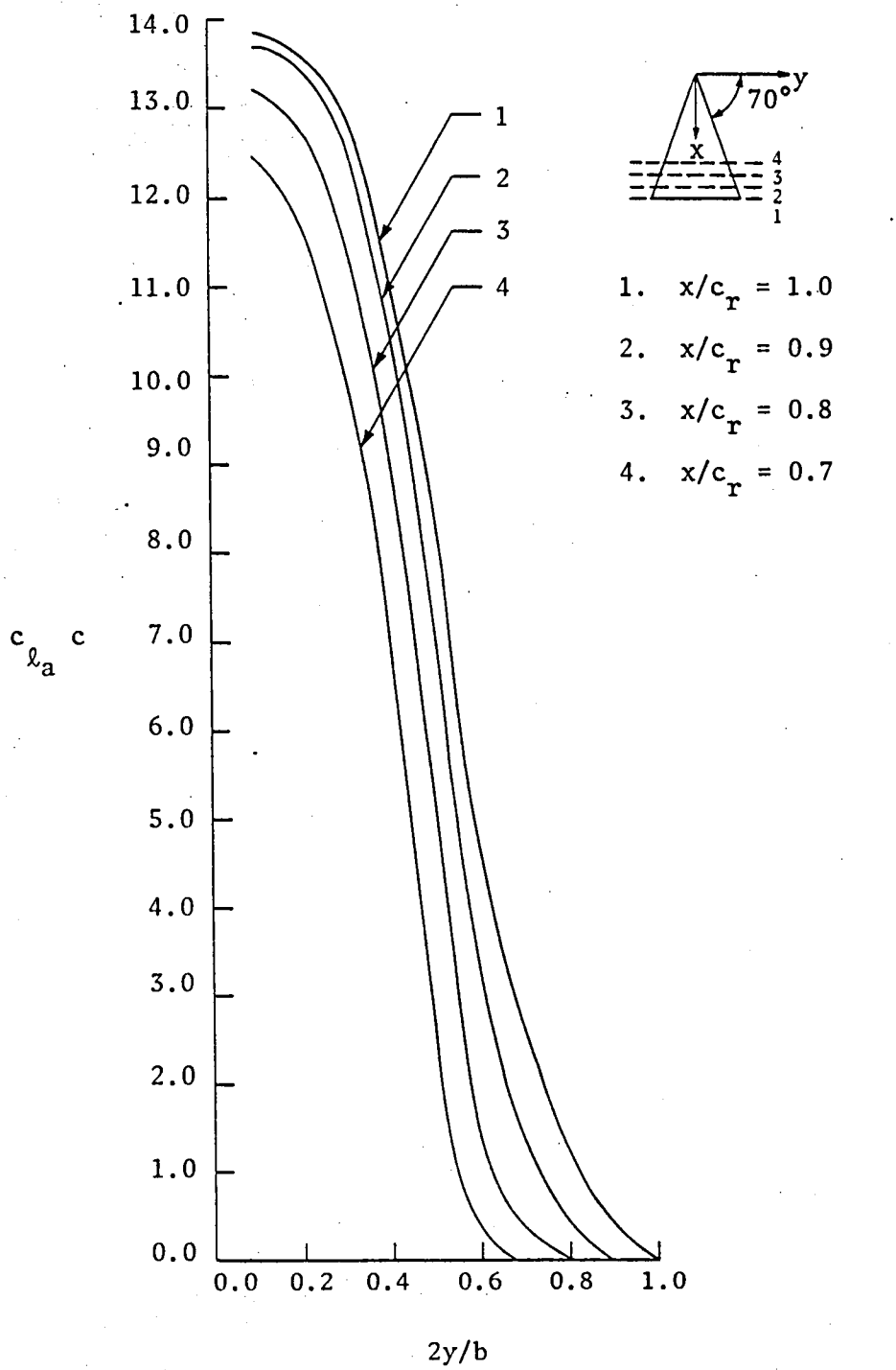

Figure 11. Accumulated span loadings for A = 1.46 flat delta wing at $\alpha = 25°$; M = 0.

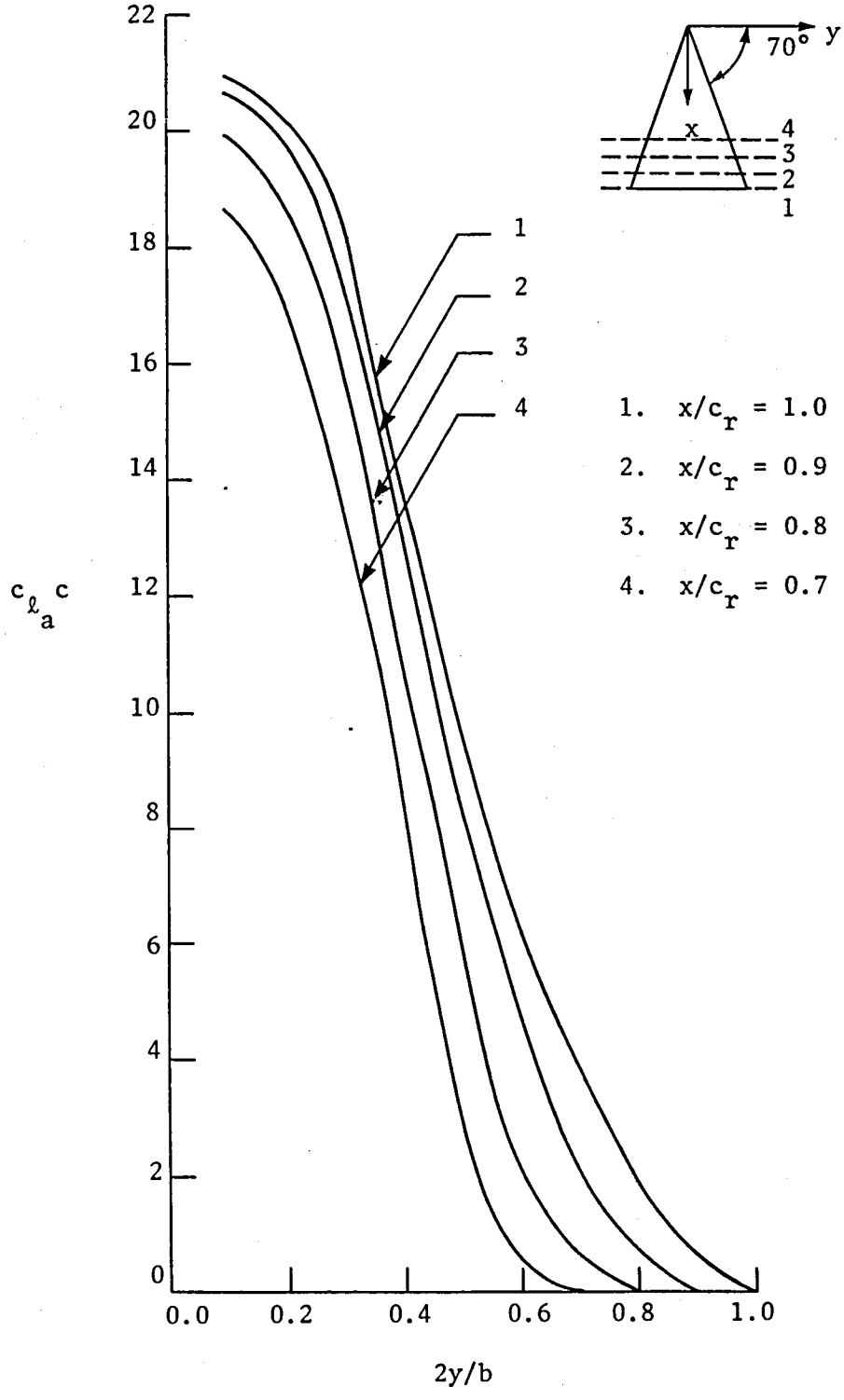

Figure 12. Accumulated span loadings for A = 1.46 flat delta wing at $\alpha = 35°$; M = 0.

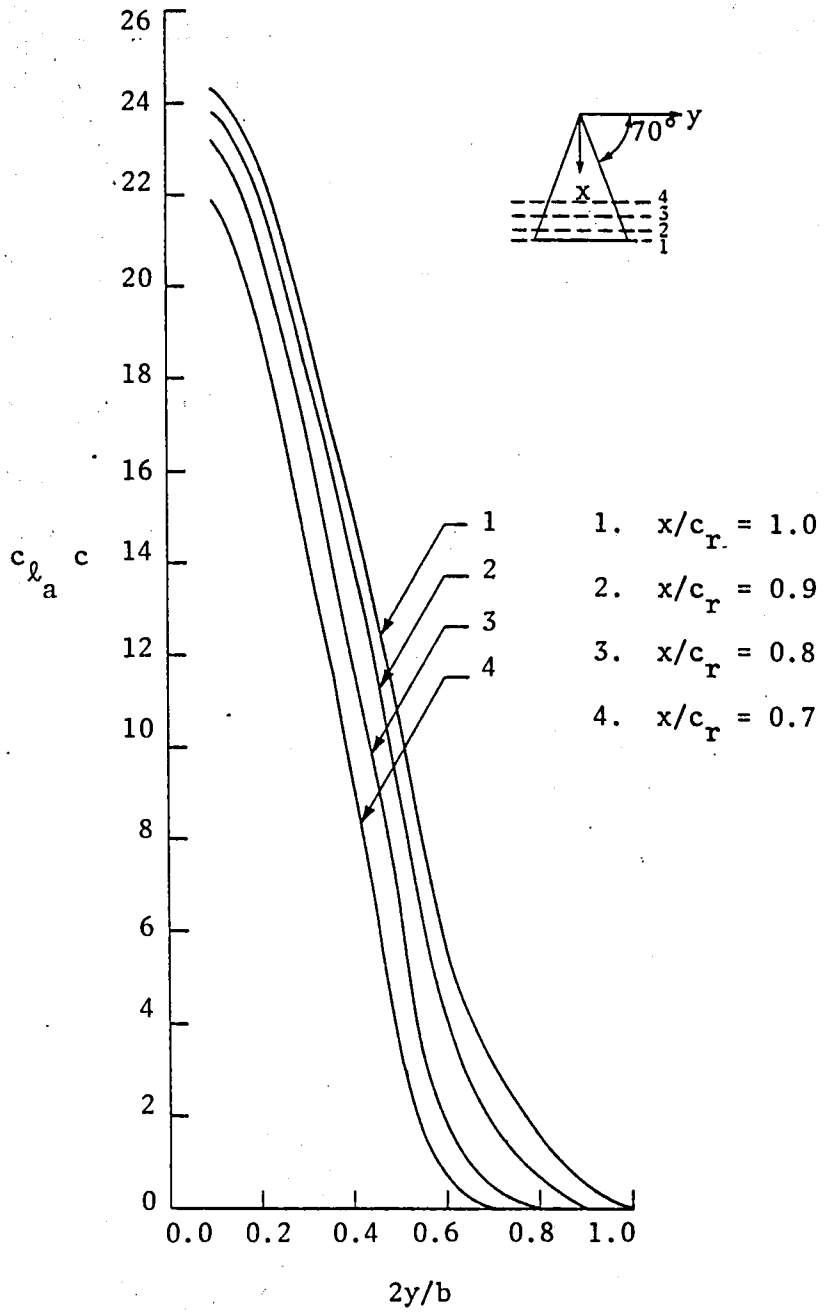

Figure 13. Accumulated span loadings for A = 1.46 flat delta wing at $\alpha = 40°$; M = 0.

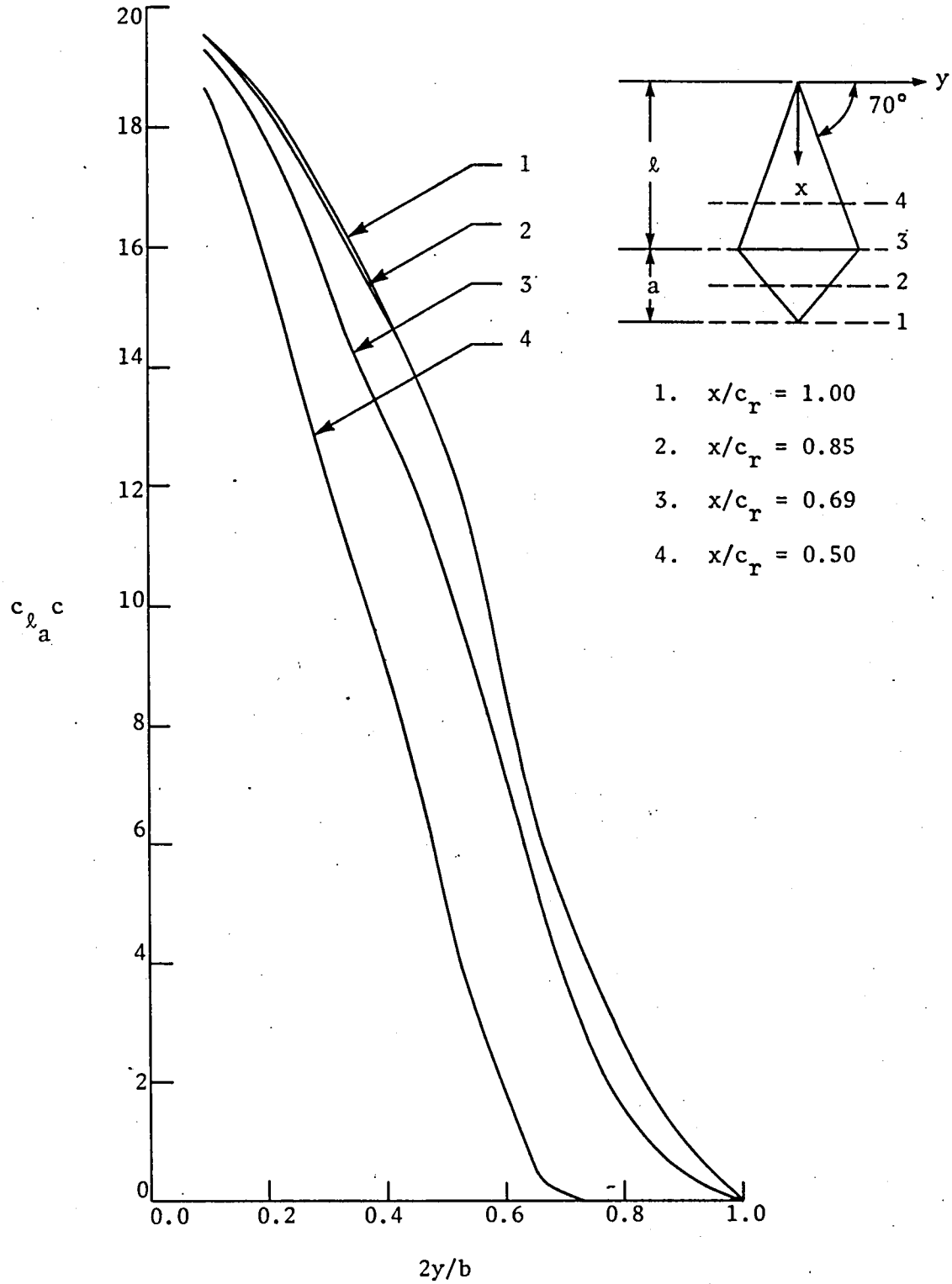

Figure 14. Accumulated span loadings for A = 1.0 flat diamond wing at $\alpha = 25°$; $\alpha/\ell = 0.455$; M = 0.

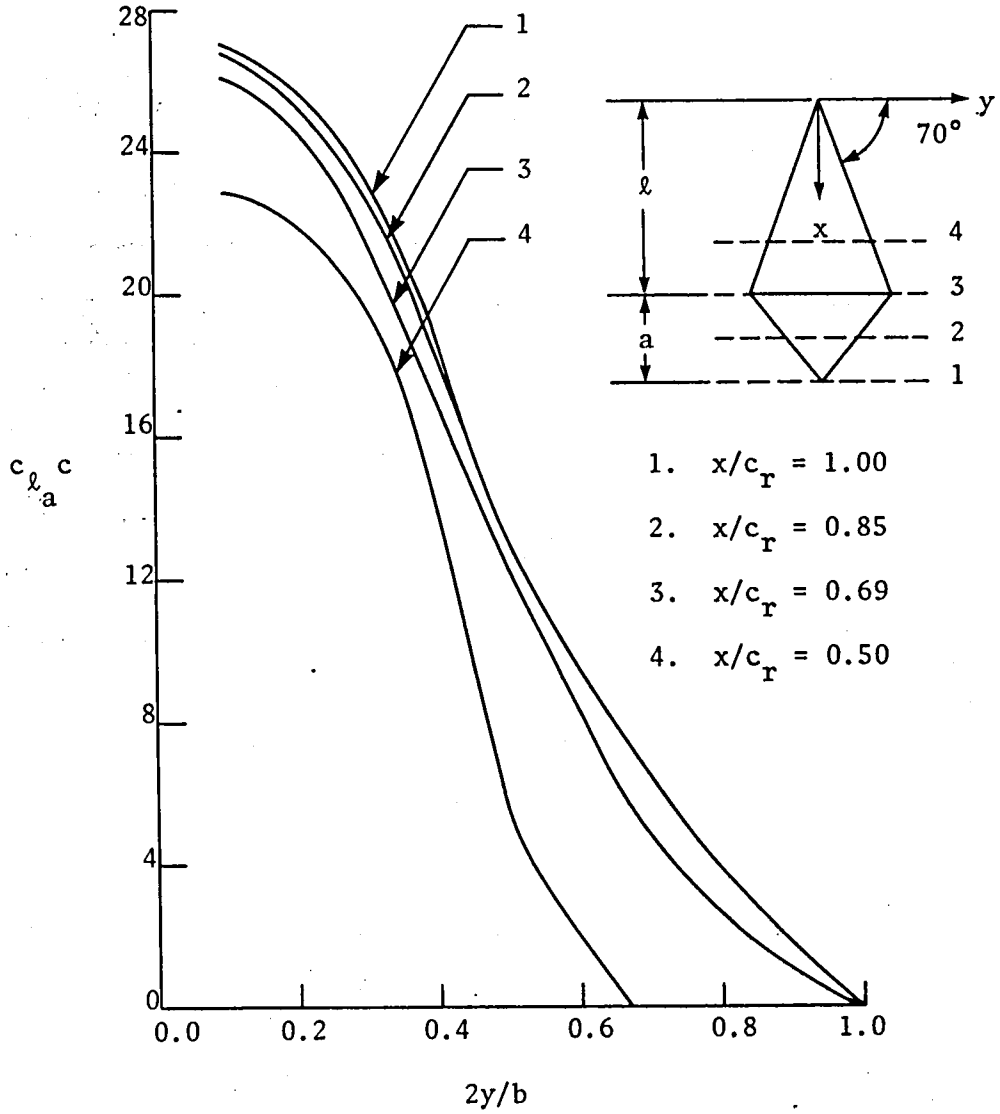

Figure 15. Accumulated span loadings for A = 1.0 flat diamond wing at $\alpha = 35°$; $\alpha/\ell = 0.455$; M = 0.

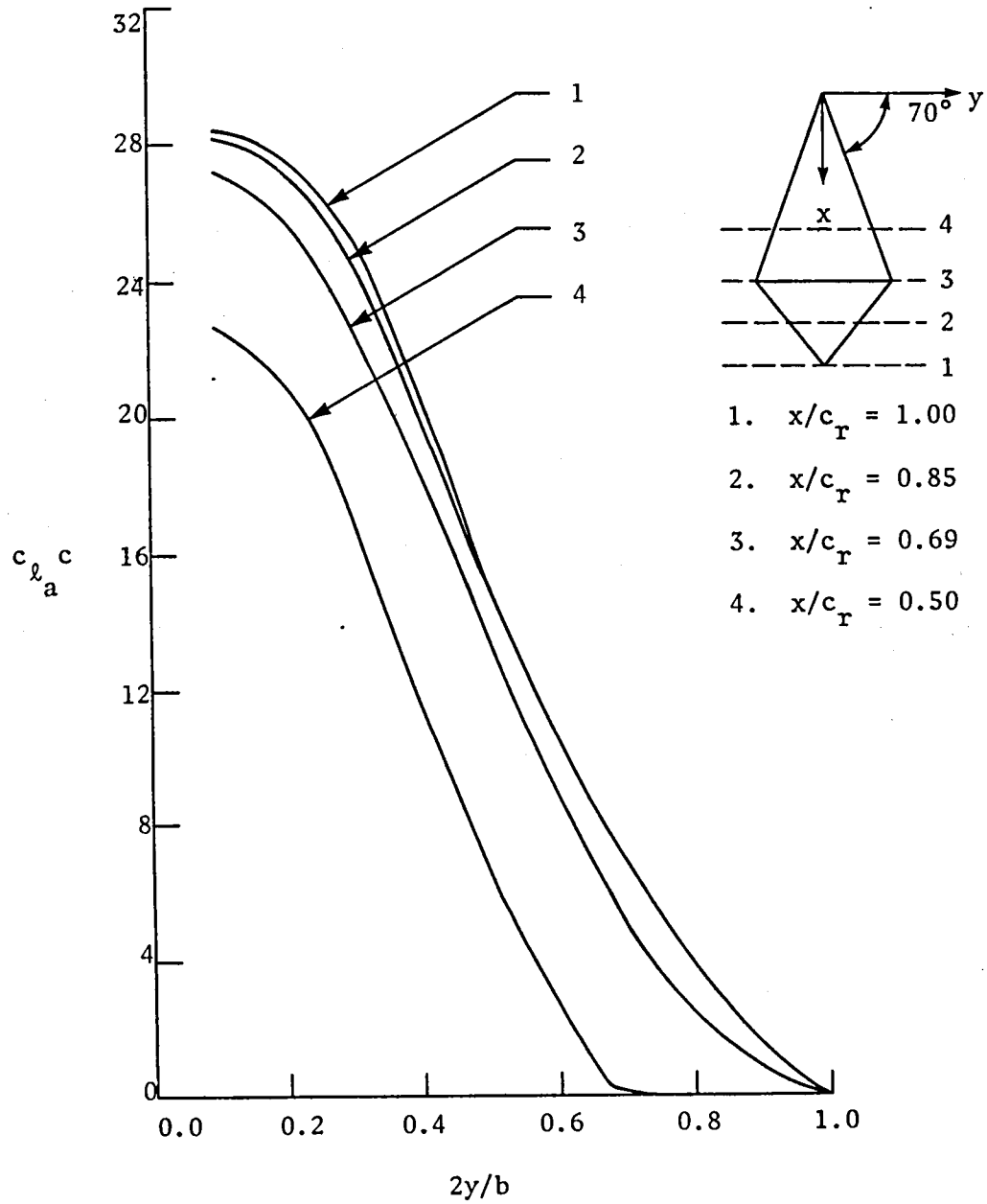

Figure 16. Accumulated span loadings for A = 1.0 flat diamond wing at α = 40; α/ℓ = 0.455; M = 0.

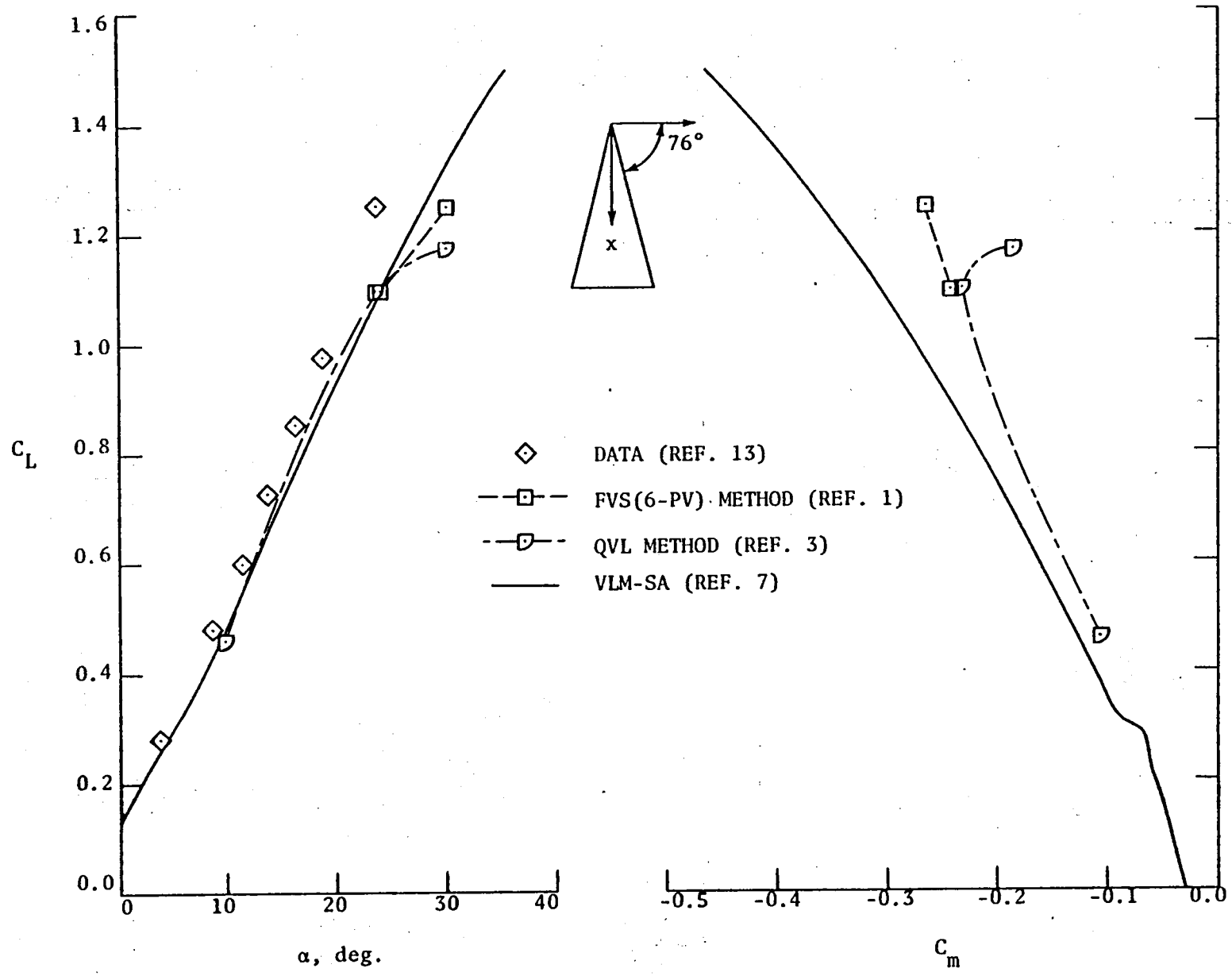

Figure 17. Lift and pitching moment coefficients for A = 1.0 chordwise cambered delta wing (Nangia's wing B); M ≈ 0.

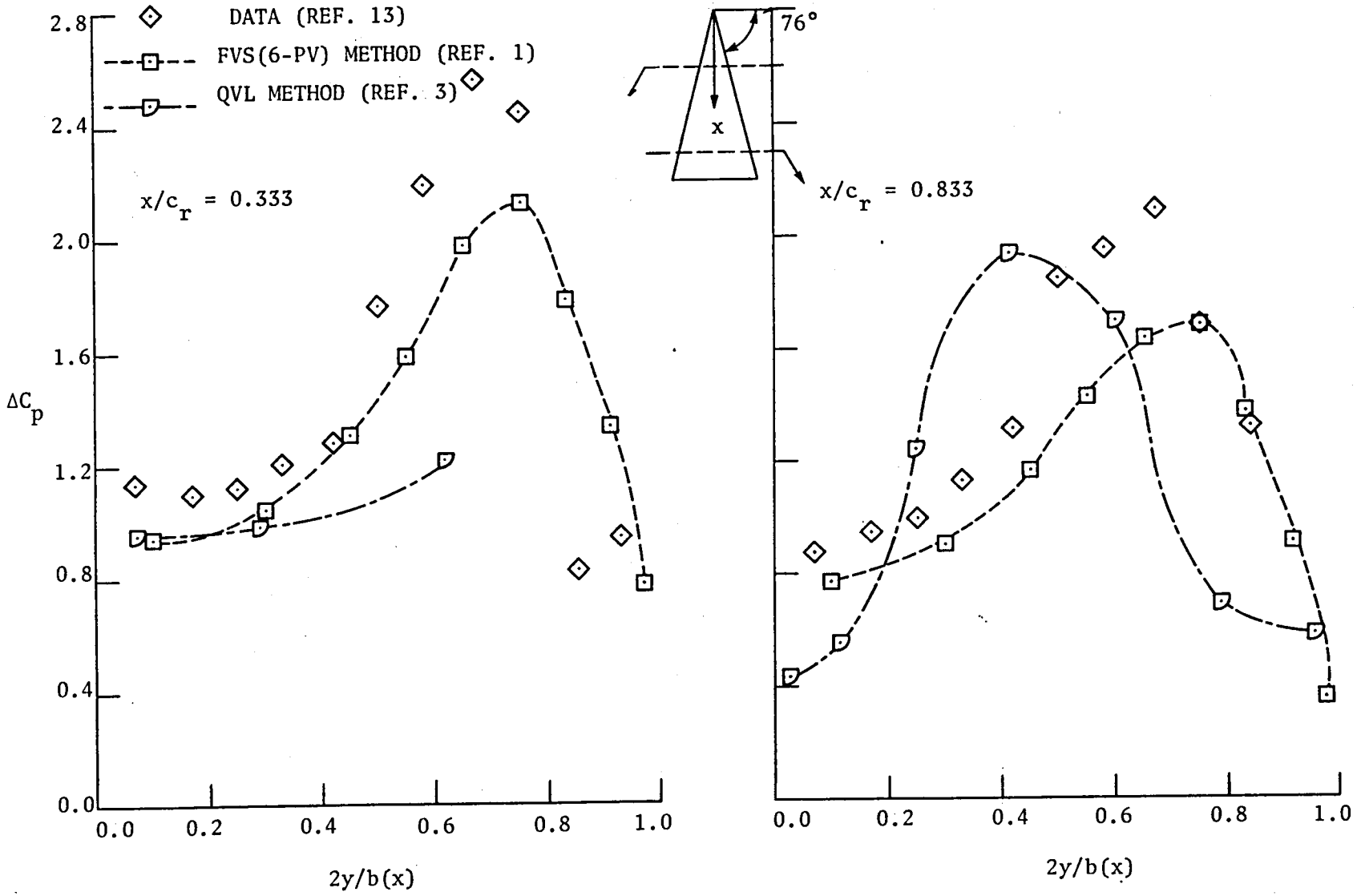

Figure 18. Spanwise pressure distributions for A = 1.0 chordwise cambered delta wing (Nangia's wing B); $\alpha = 23.8°$; $M \simeq 0$.

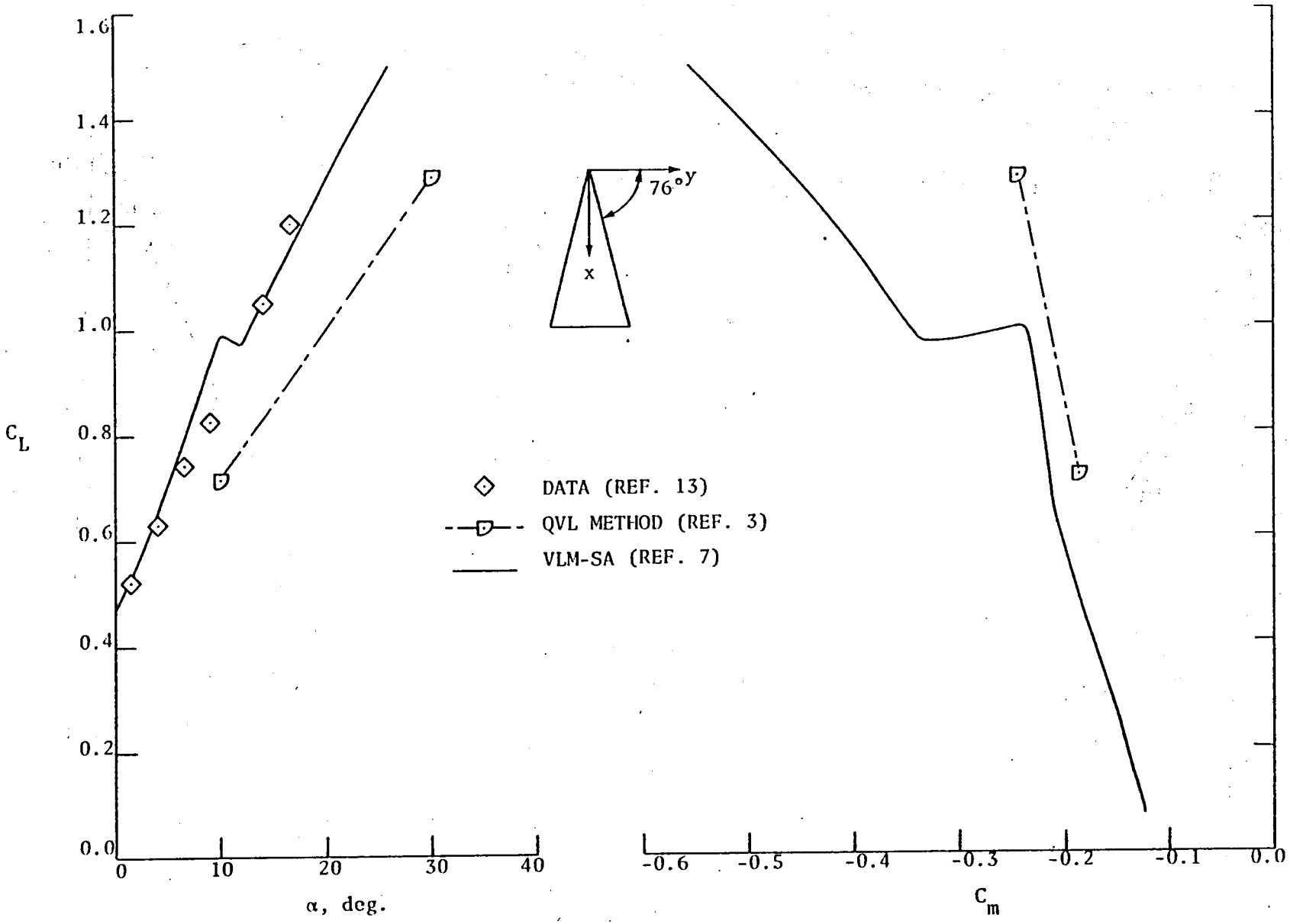

Figure 19. Variation of lift and pitching moment coefficients for A = 1.0 chordwise cambered delta wing (Nangia's wing C); M ≈ 0.

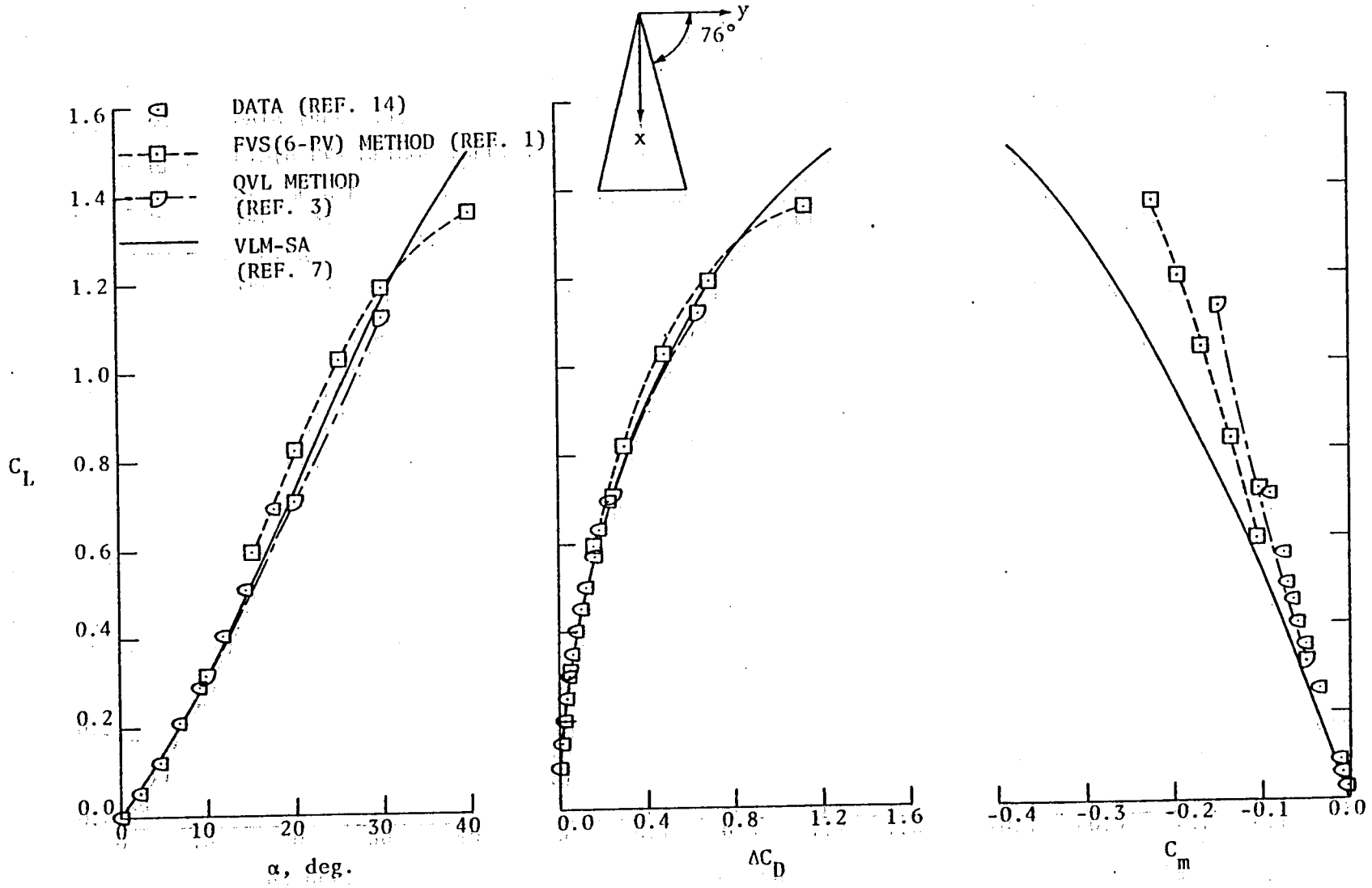

Figure 20. Longitudinal aerodynamic characteristics of A = 1.0 Squire's spanwise cambered delta wing 4; M ≈ 0.

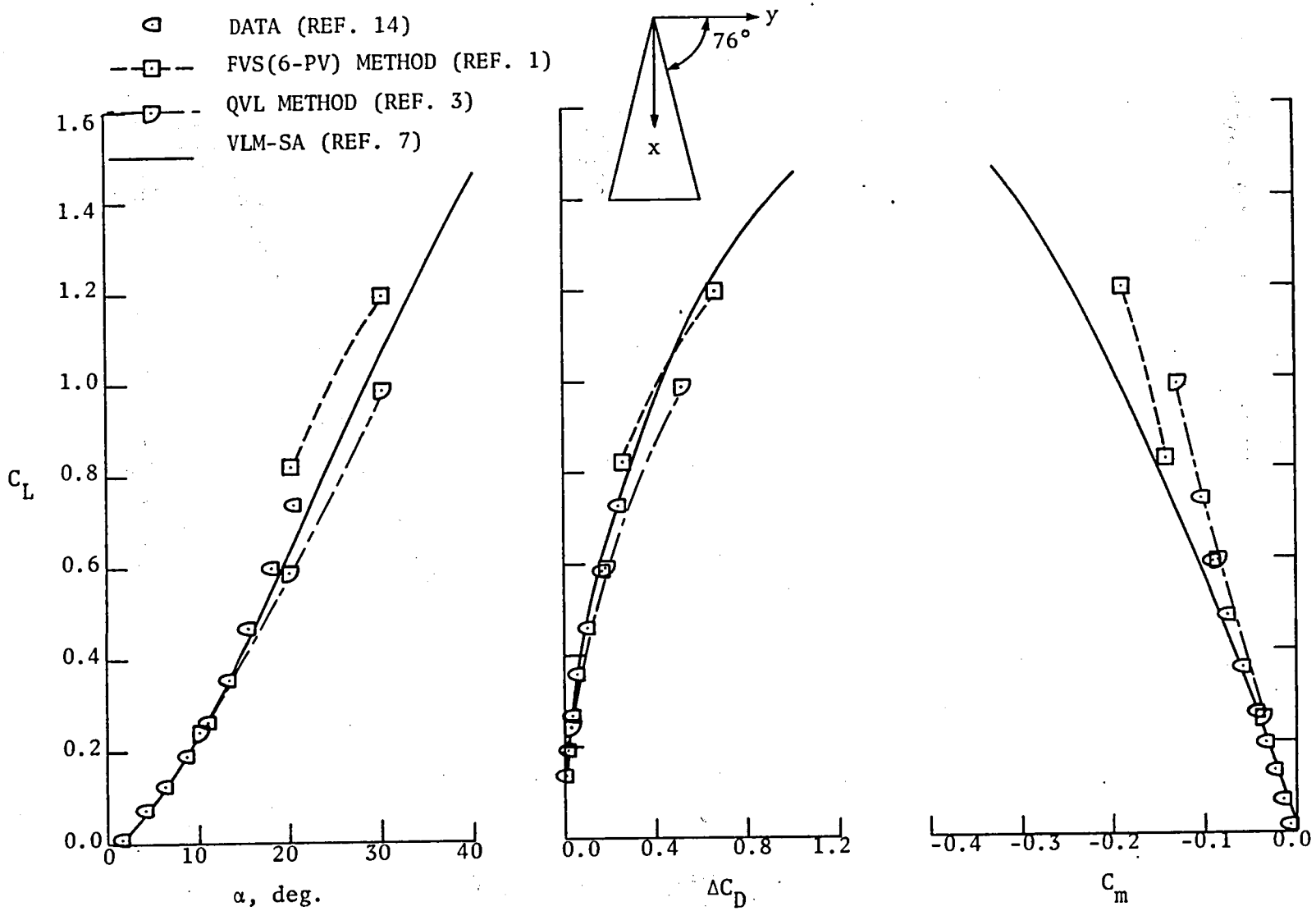

Figure 21. Longitudinal aerodynamic characteristics of A = 1.0 Squire's spanwise cambered delta wing-5; M ≈ 0.

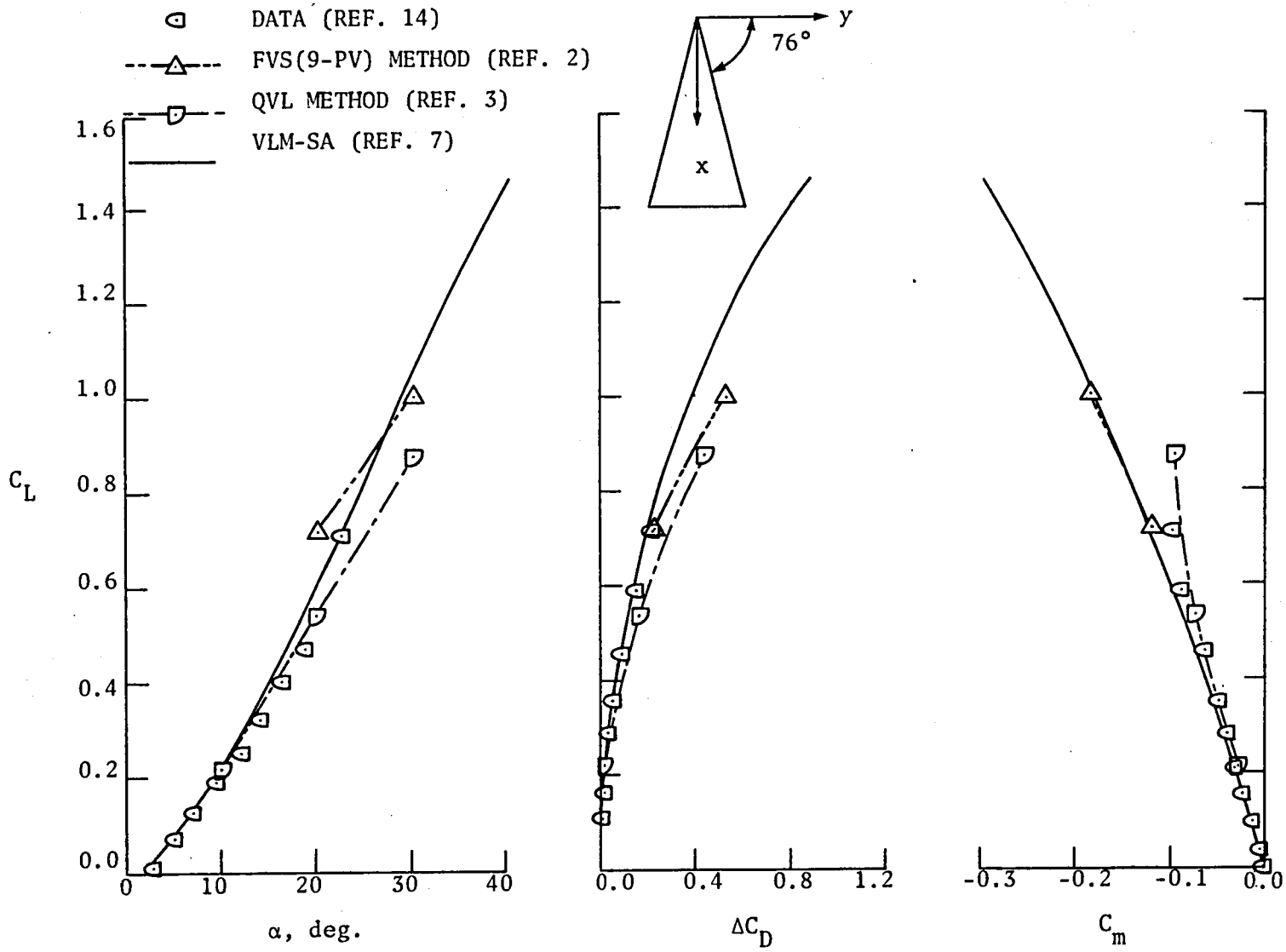

Figure 22. Longitudinal aerodynamic characteristics of A = 1.0 Squire's spanwise cambered delta wing-6; M ≈ 0.

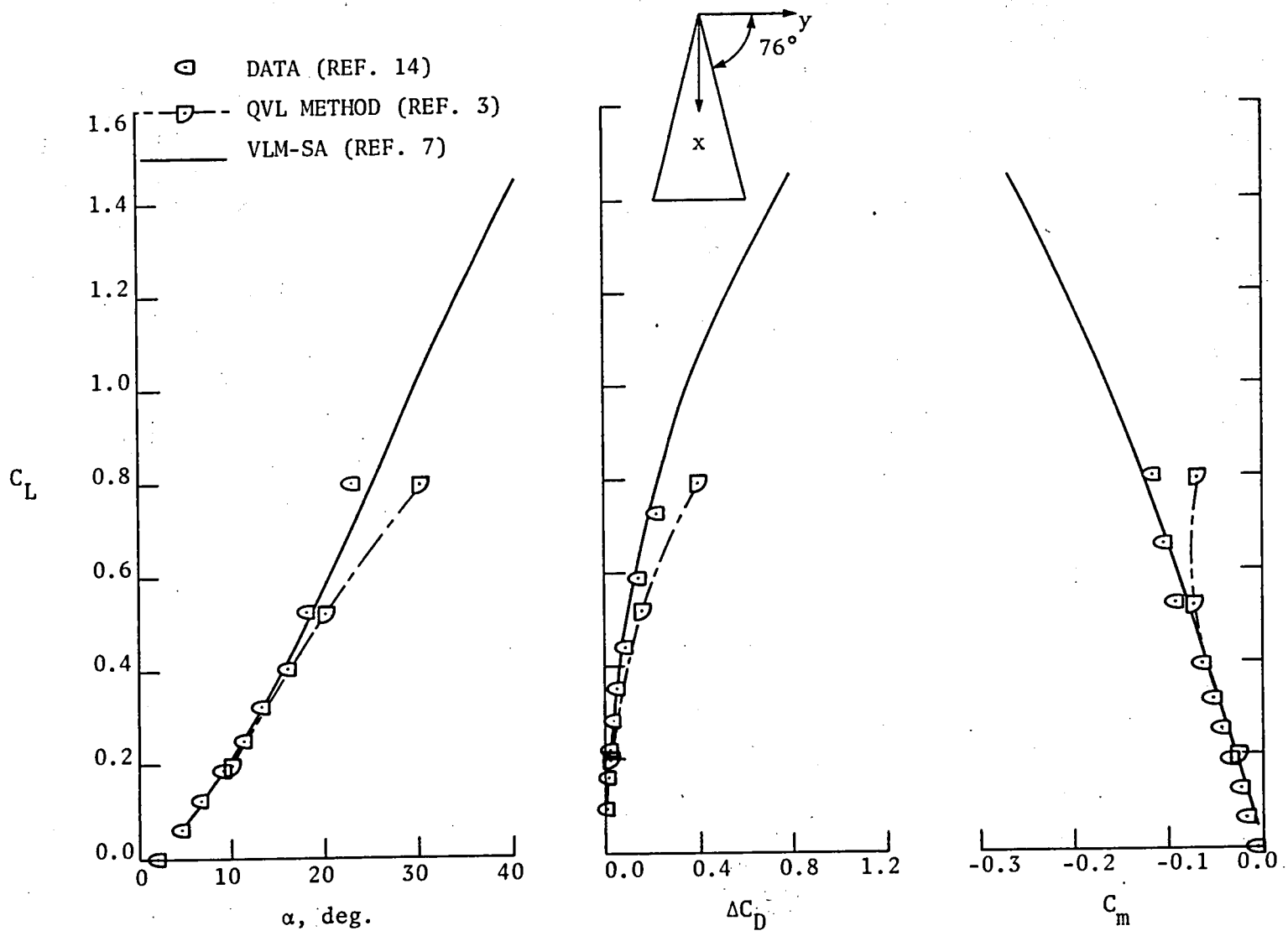

Figure 23. Longitudinal aerodynamic characteristics of A = 1.0 Squire's spanwise cambered delta wing-7; M ≈ 0.

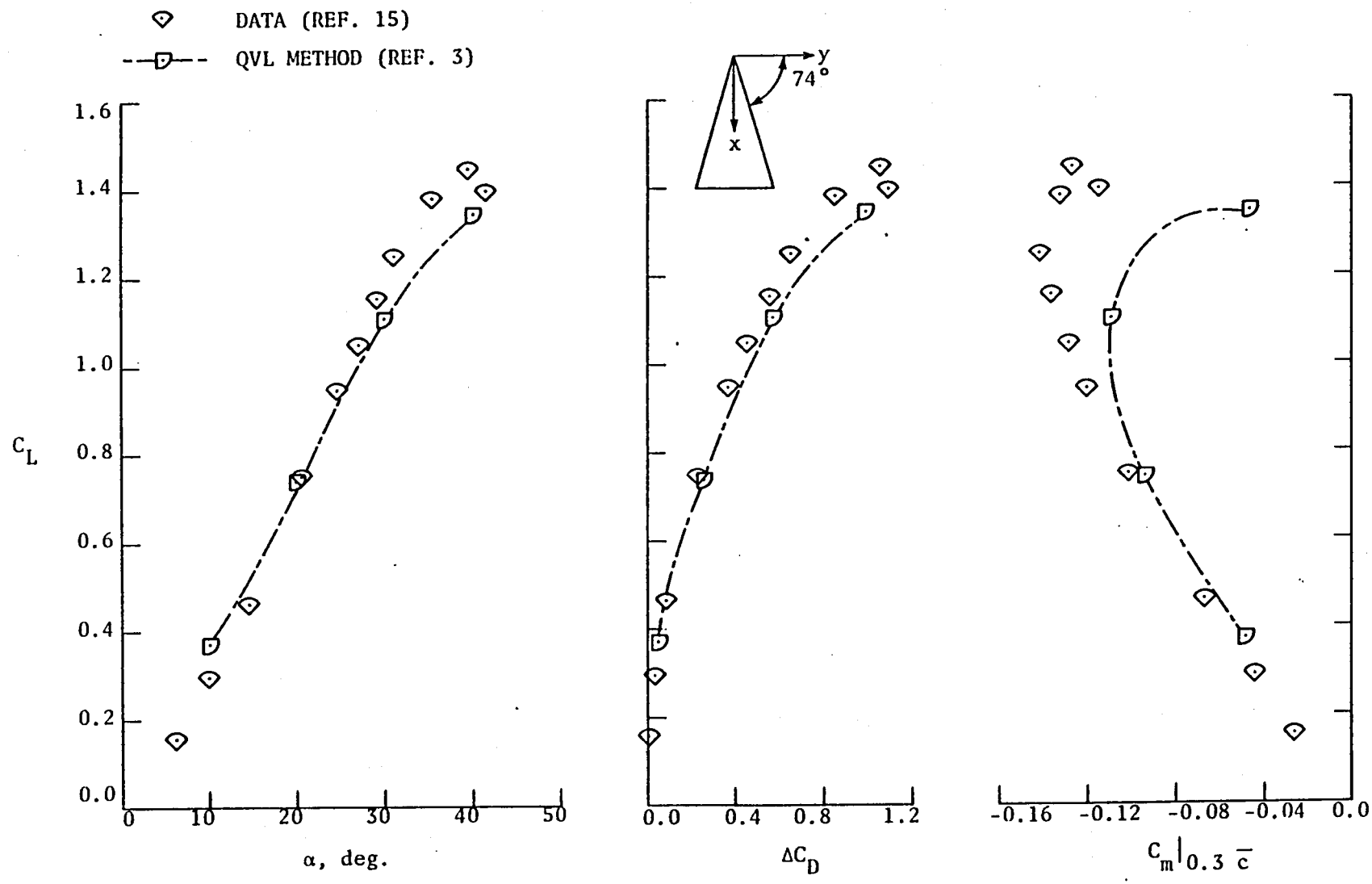

Figure 24. Longitudinal aerodynamic characteristics of A = 1.15 apex cambered delta wing; M ≈ 0.

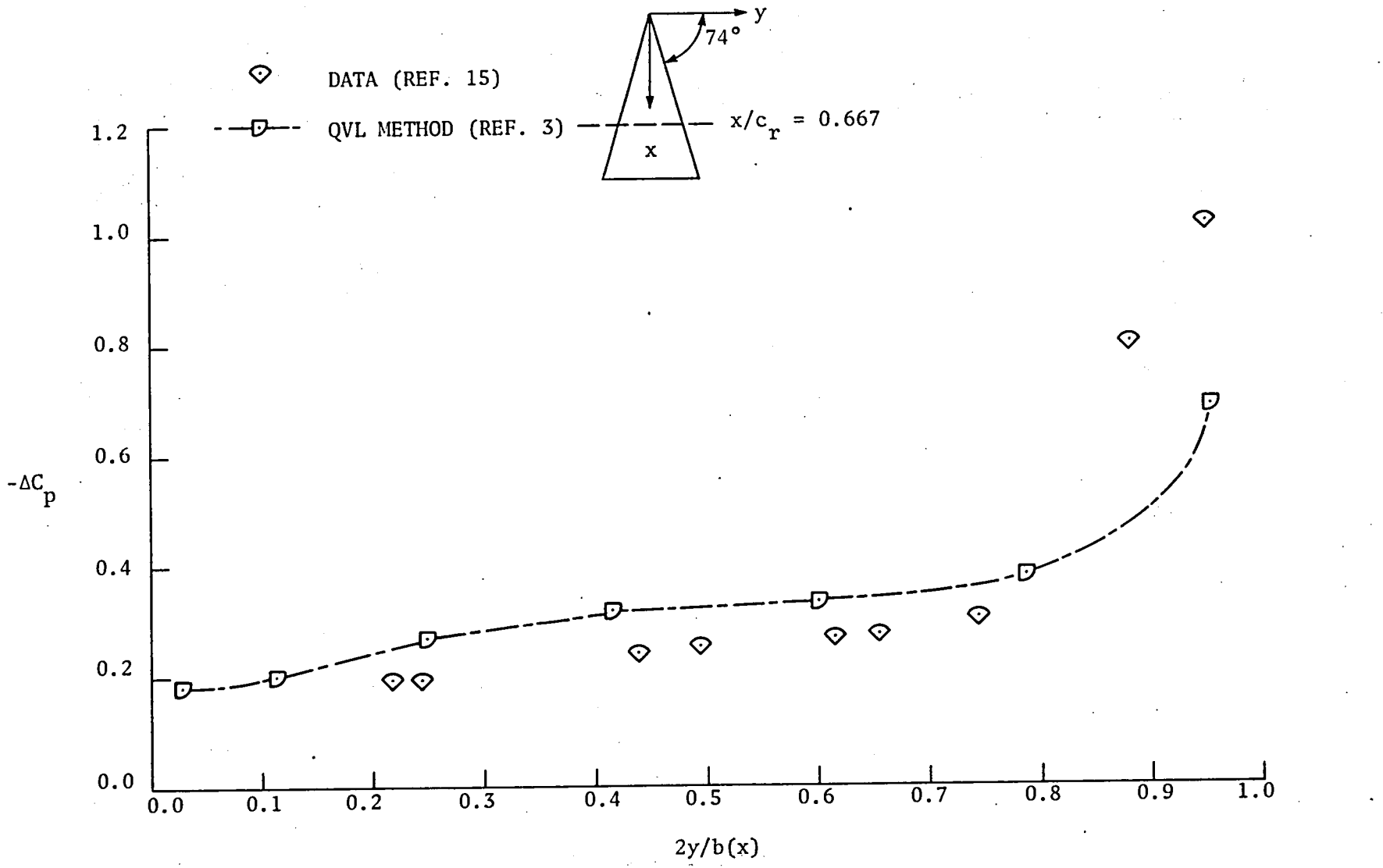

Figure 25. Spanwise pressure distribution for A = 1.15 apex cambered delta wing at $\alpha = 10°$; M ≈ 0.

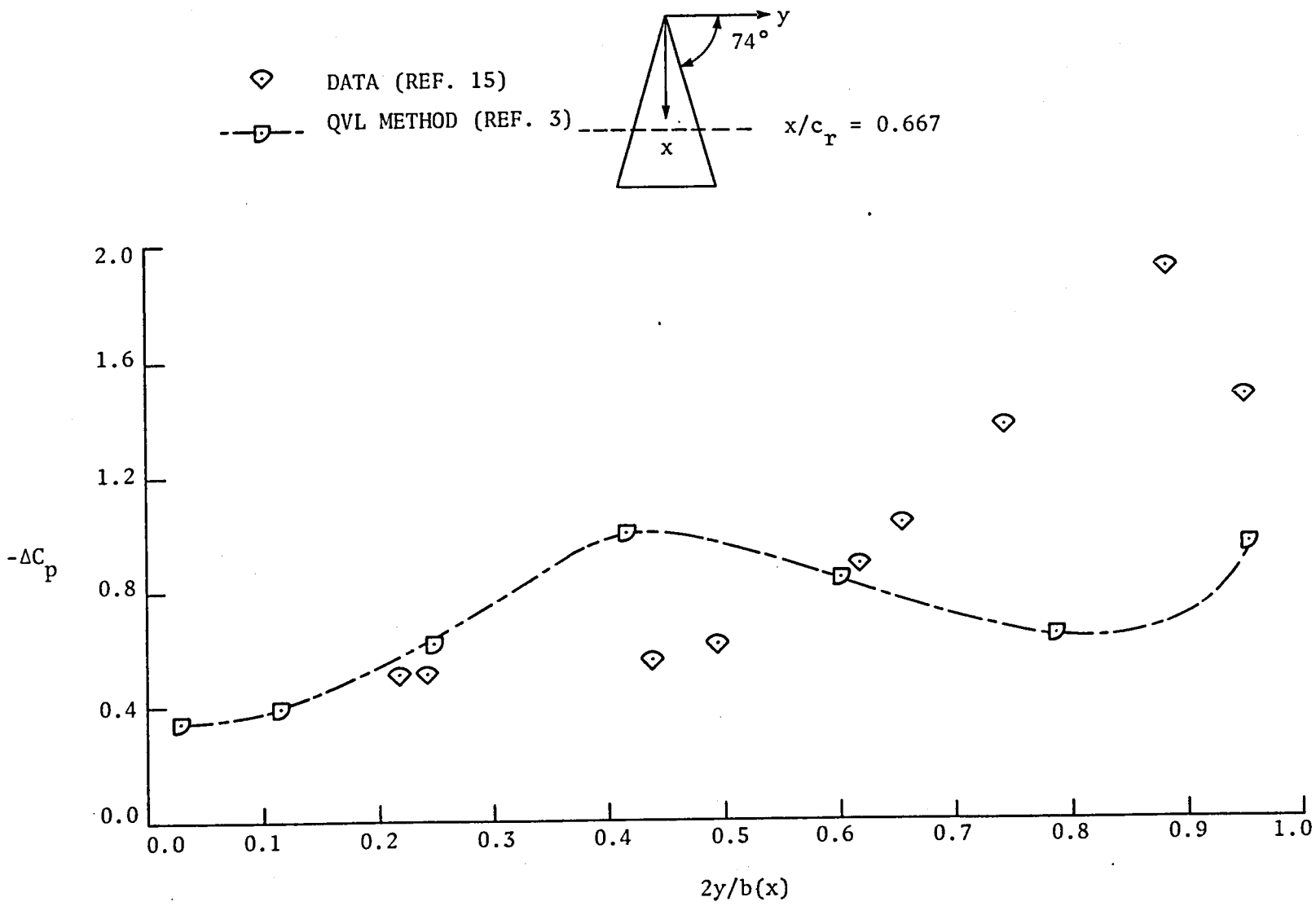

Figure 26. Spanwise pressure distribution for A = 1.15 apex cambered delta wing at $\alpha = 20°$; $M \simeq 0$.

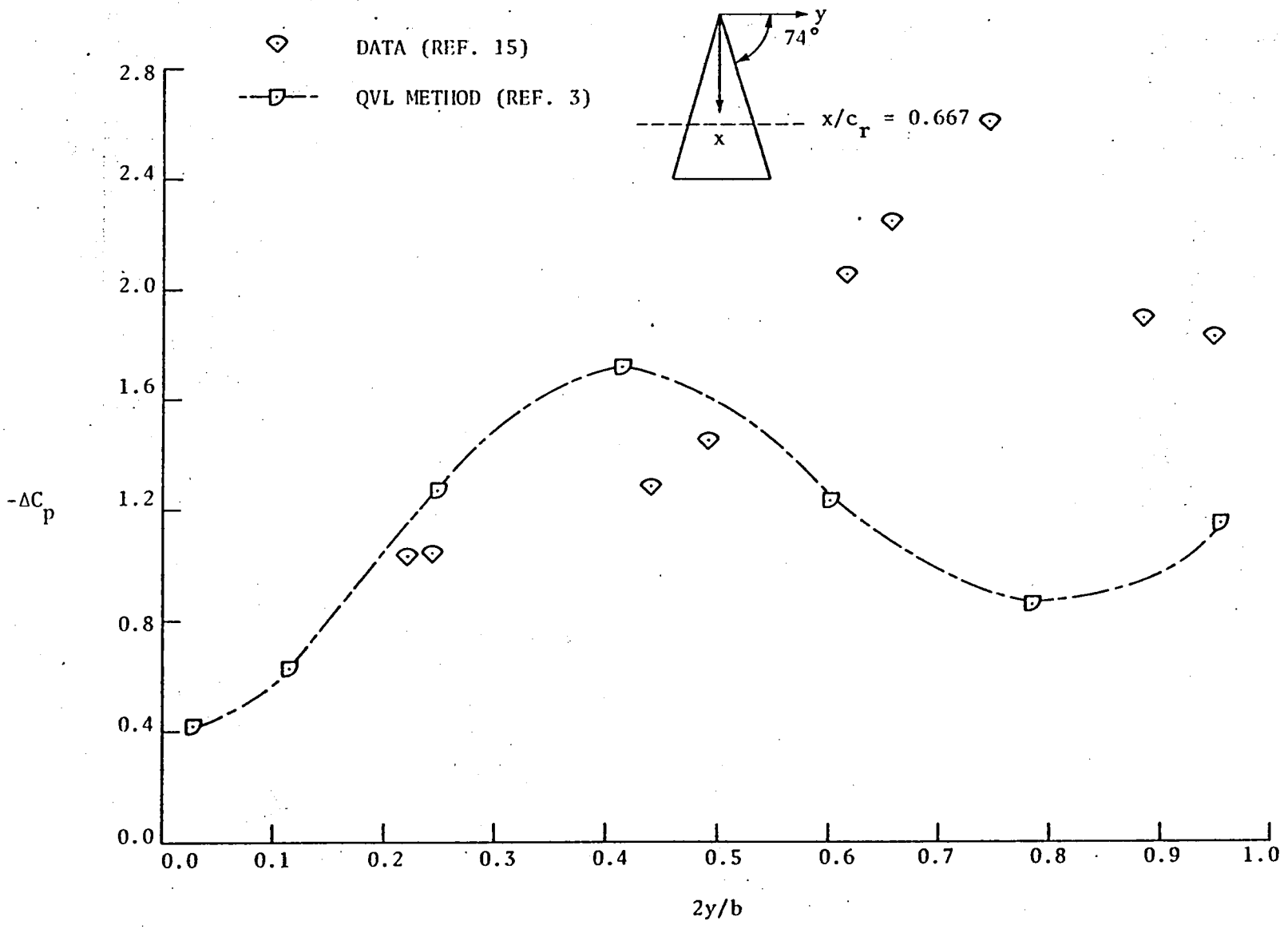

Figure 27. Spanwise pressure distribution for A = 1.15 apex cambered delta wing at $\alpha = 30°$; $M \simeq 0$.

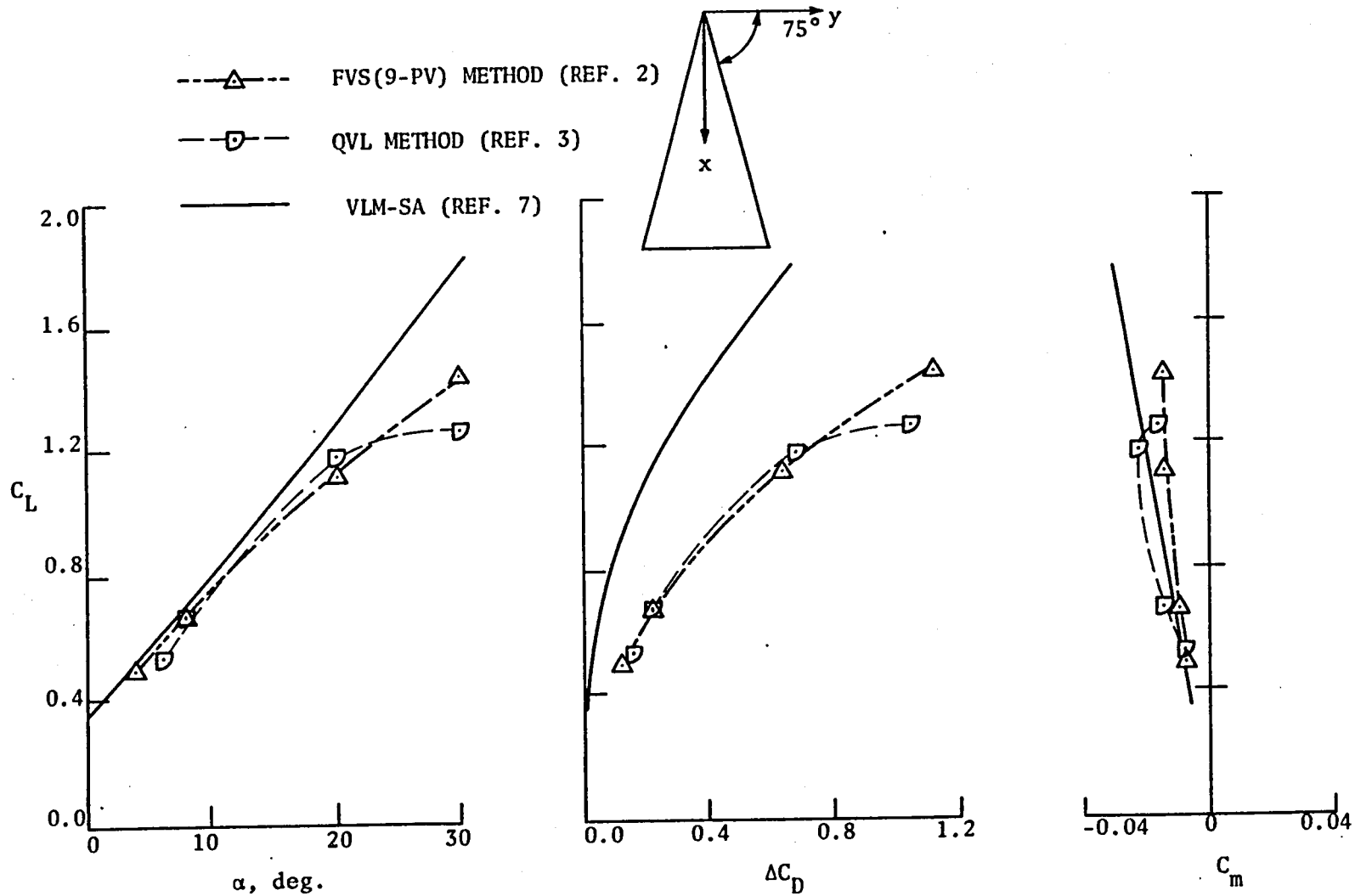

Figure 28. Longitudinal aerodynamic characteristics of A = 1.07 cambered delta wing designed for C_{L_D} = 0.3 with smooth onflow; M = 0.

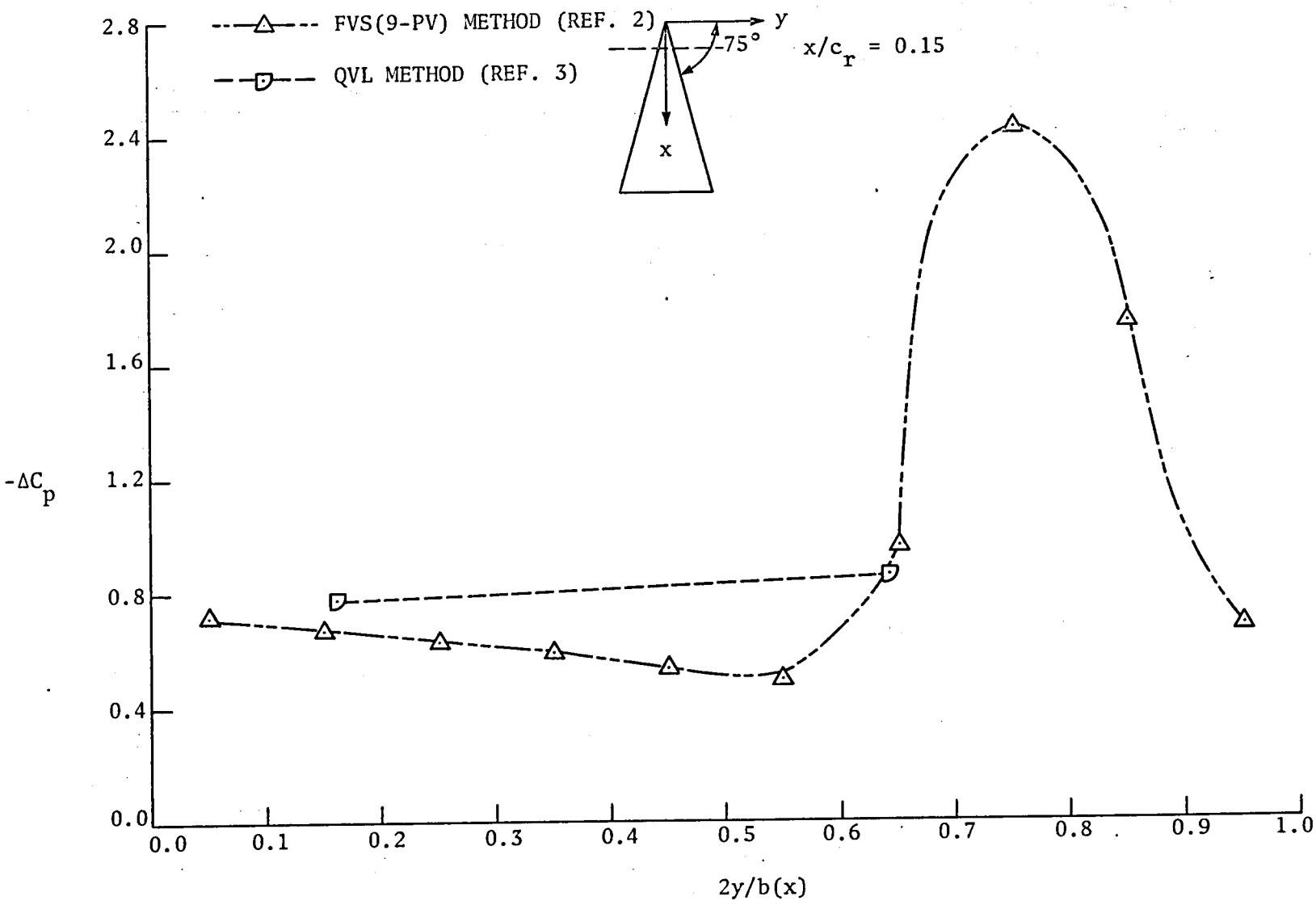

Figure 29. Spanwise pressure distribution at $x/c_r = 0.15$ for A = 1.07 cambered delta wing designed for $C_{L_D} = 0.3$ with smooth onflow; $\alpha = 6.3°$; M = 0.

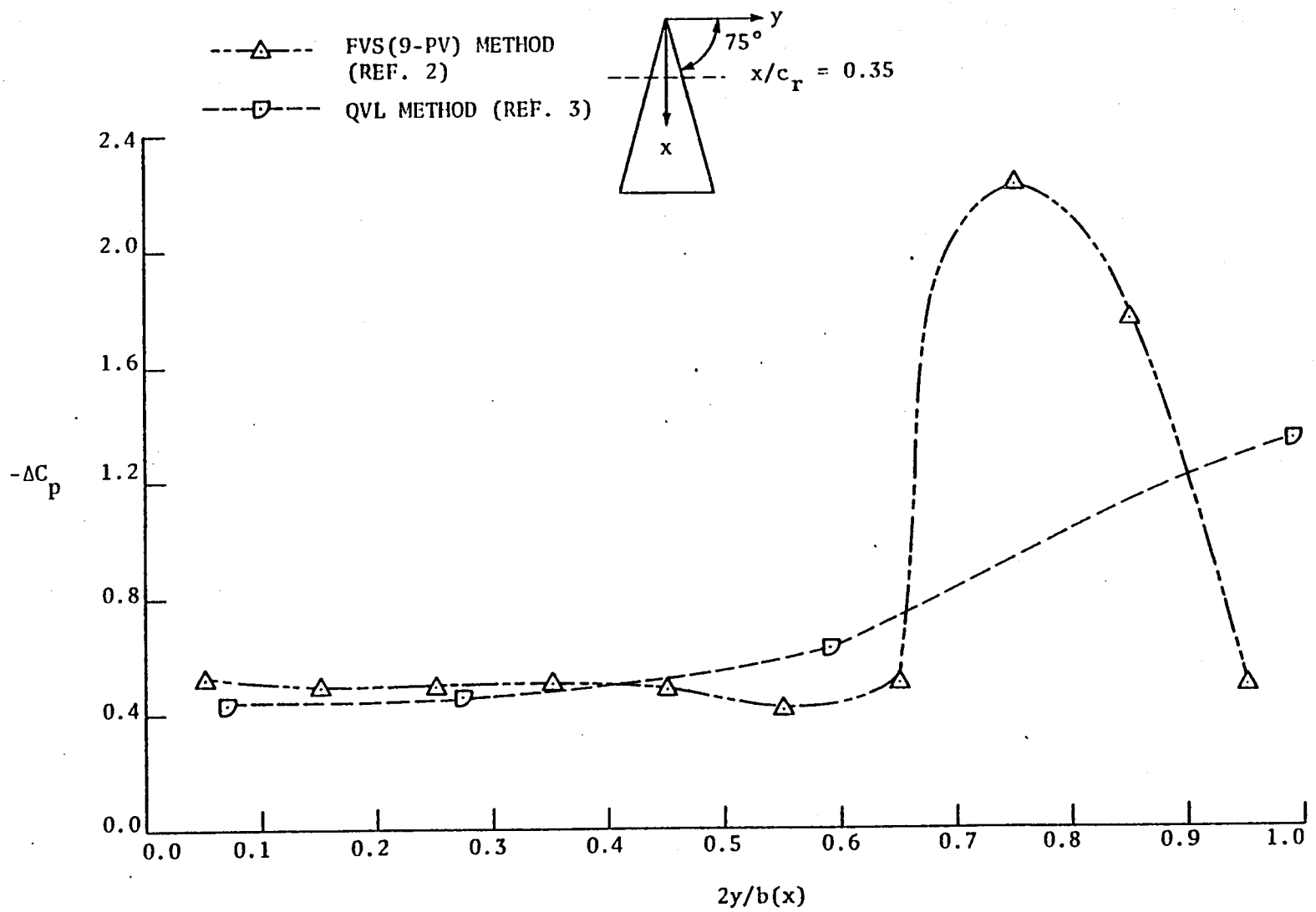

Figure 30. Spanwise pressure distribution at $x/c_r = 0.35$ for A = 1.07 cambered delta wing designed for $C_{L_D} = 0.3$ with smooth onflow; $\alpha = 6.3°$; M = 0.

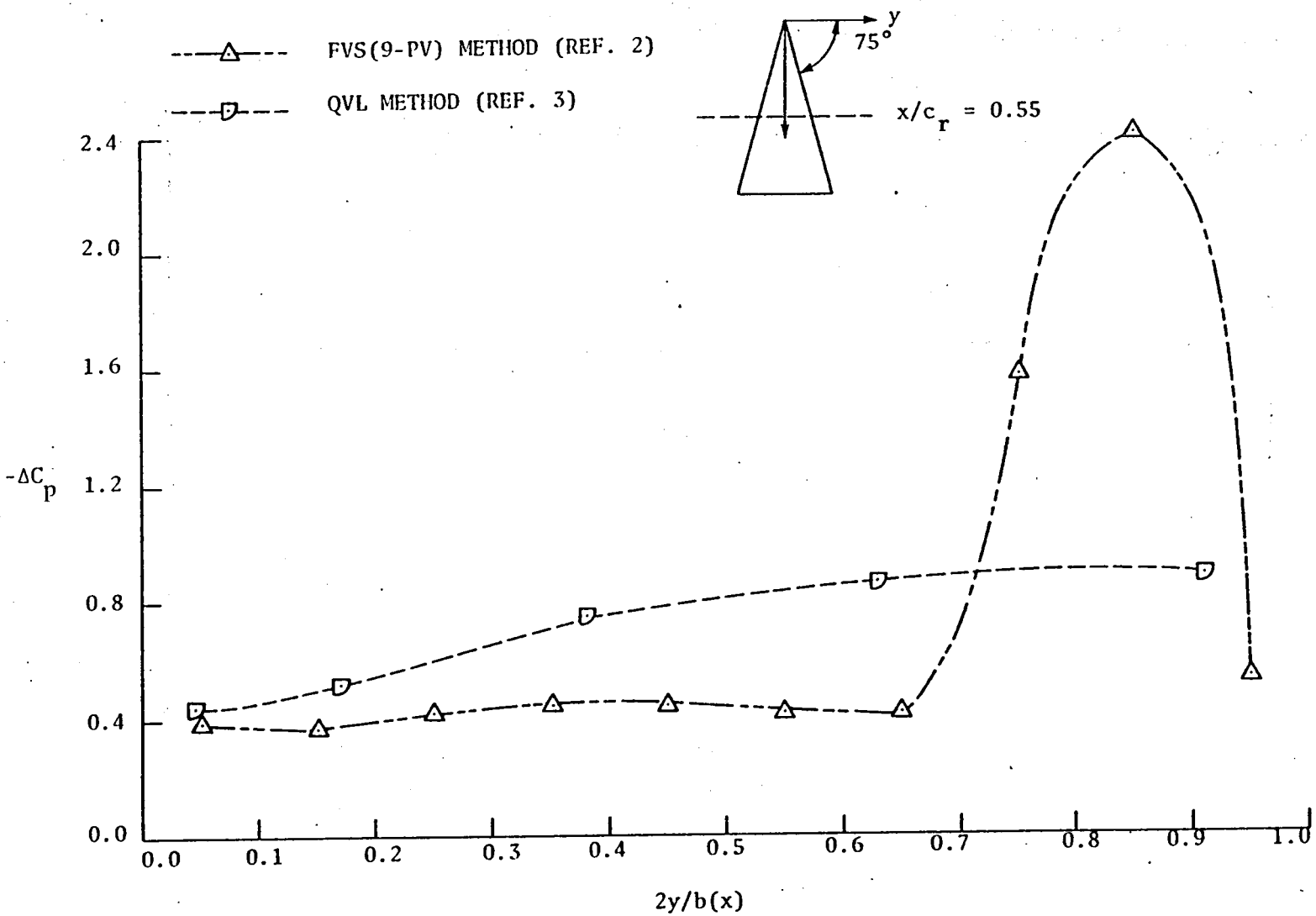

Figure 31. Spanwise pressure distribution at $x/c_r = 0.55$ for A = 1.07 cambered delta wing designed for $C_{L_D} = 0.3$ with smooth onflow; $\alpha = 6.3°$; M = 0.

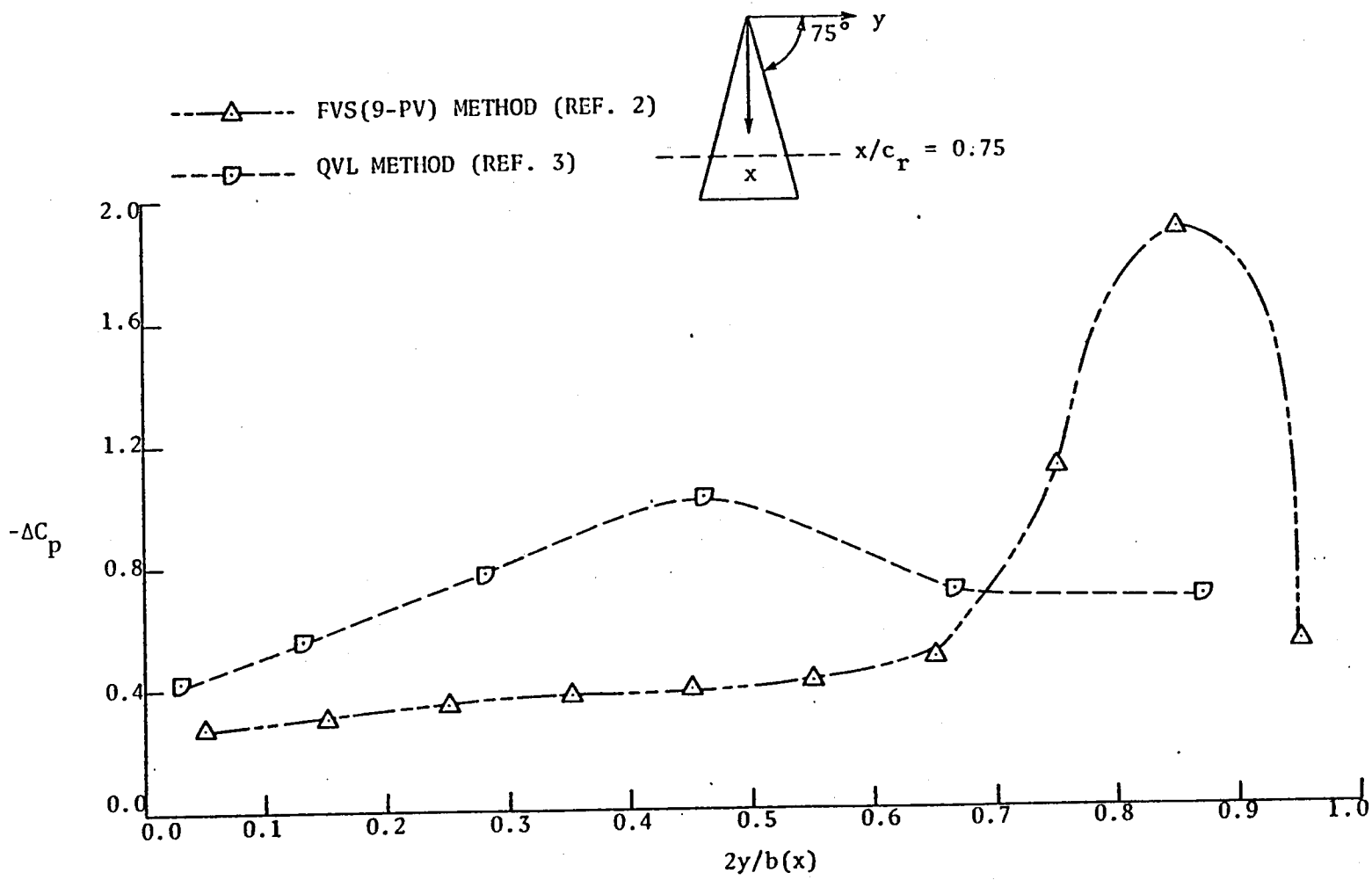

Figure 32. Spanwise pressure distribution at $x/c_r = 0.75$ for A = 1.07 cambered delta wing designed for $C_{L_D} = 0.3$ with smooth onflow; $\alpha = 6.3°$; M = 0.

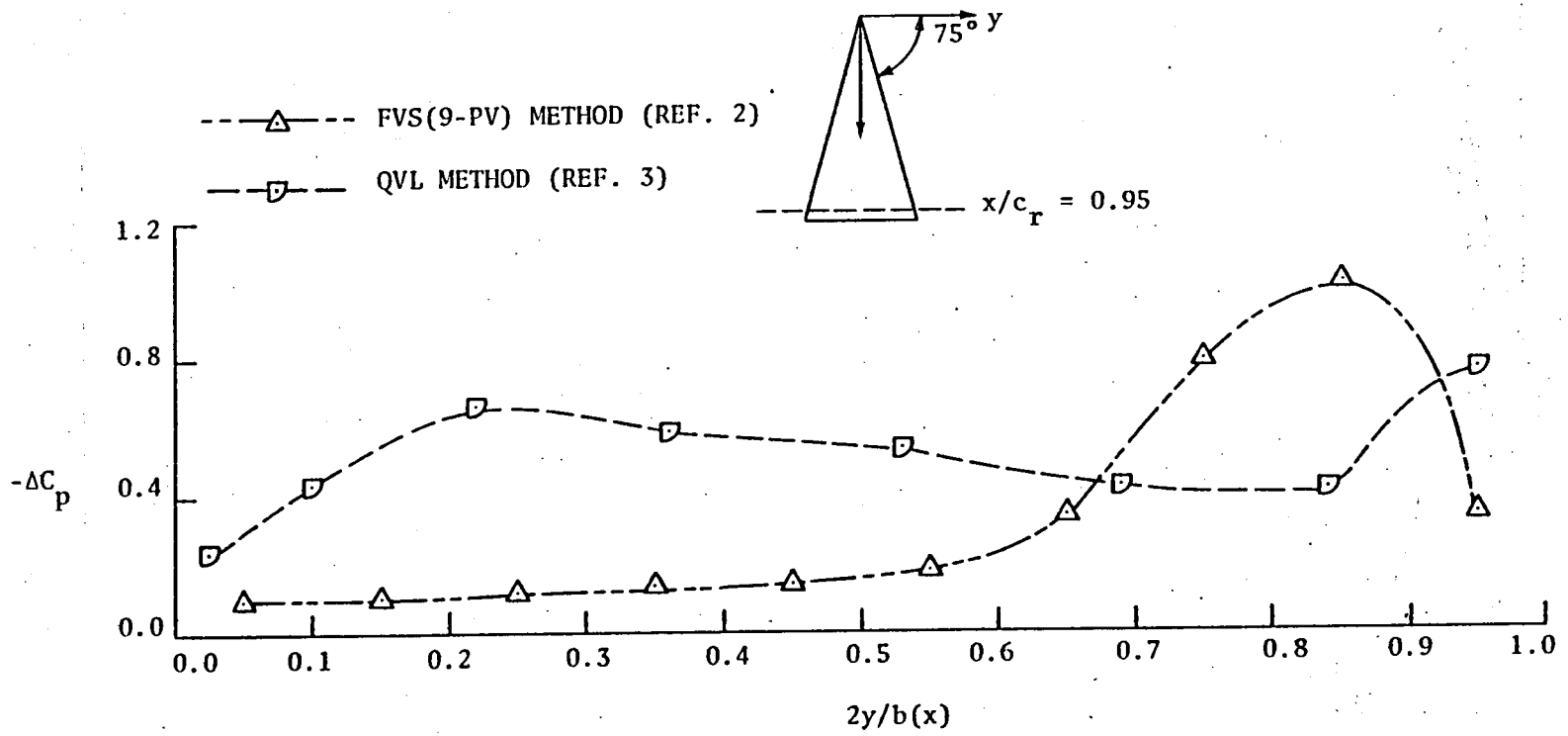

Figure 33. Spanwise pressure distribution at $x/c_r = 0.95$ for A = 1.07 cambered delta wing designed for $C_{L_D} = 0.3$ with smooth onflow; $\alpha = 6.3°$; M = 0.

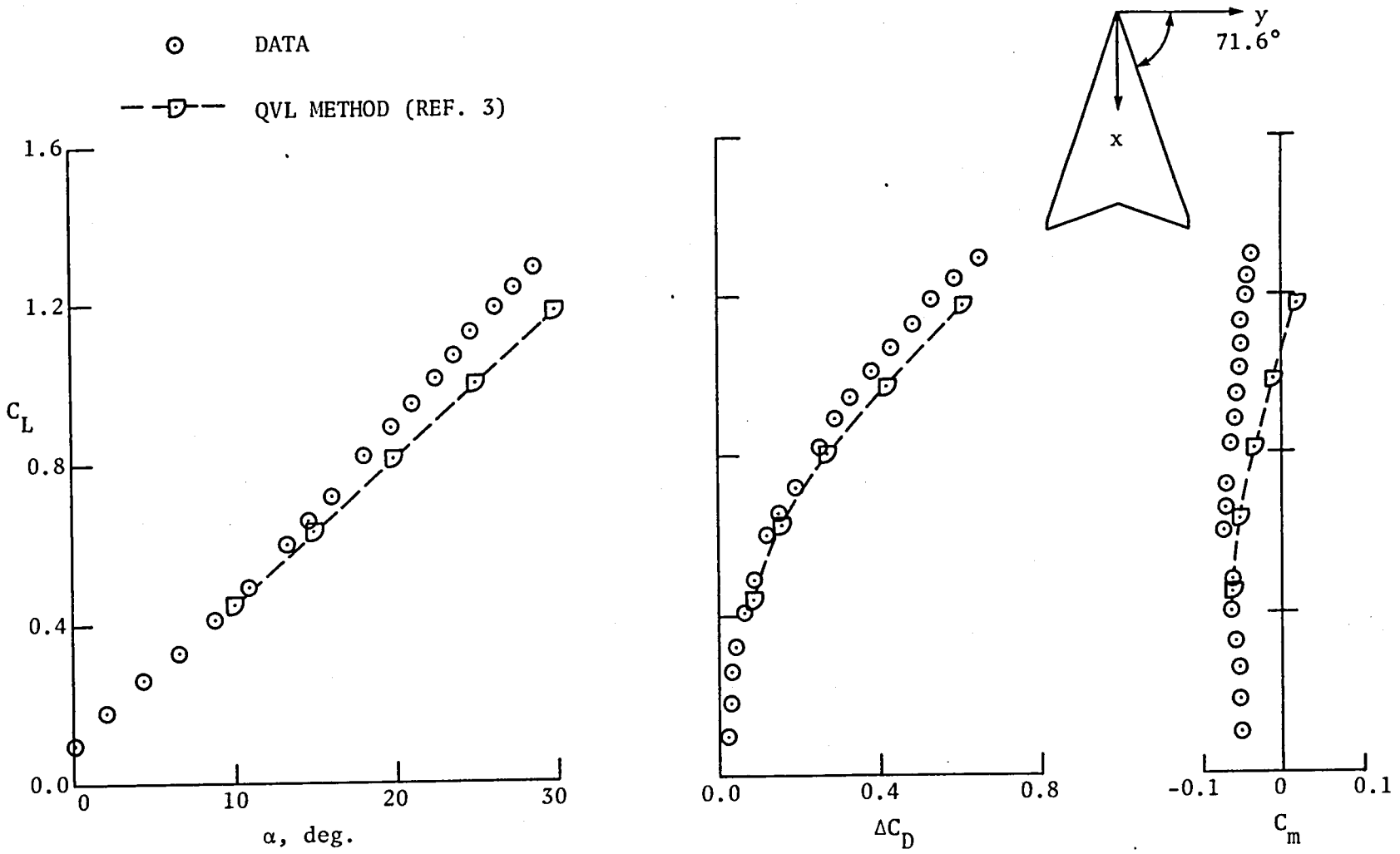

Figure 34. Longitudinal aerodynamic characteristics of A = 1.51 cambered cropped arrow wing; M = 0.6.

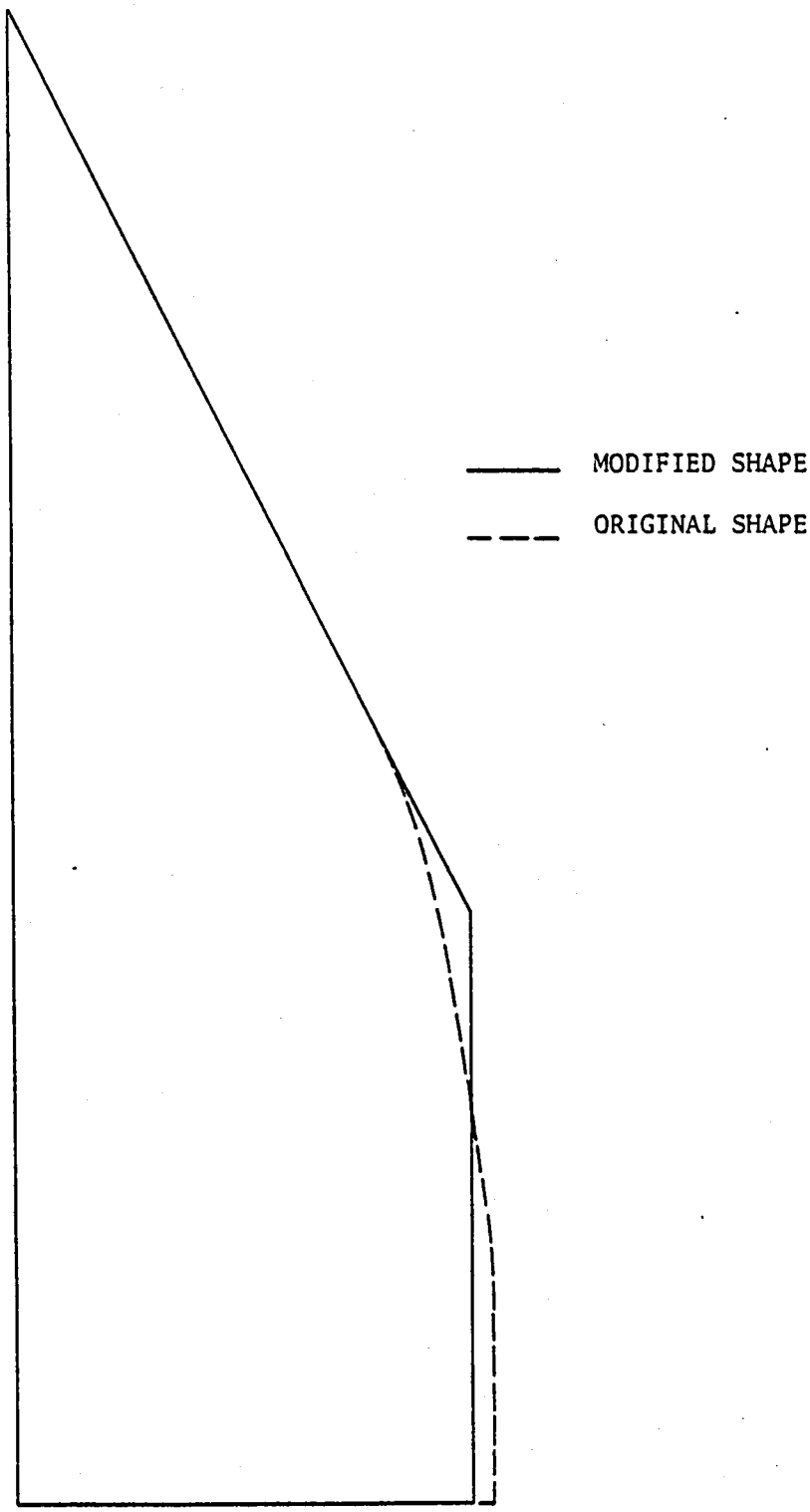

Figure 35. Planforms of modified and unmodified flat cropped delta wing.

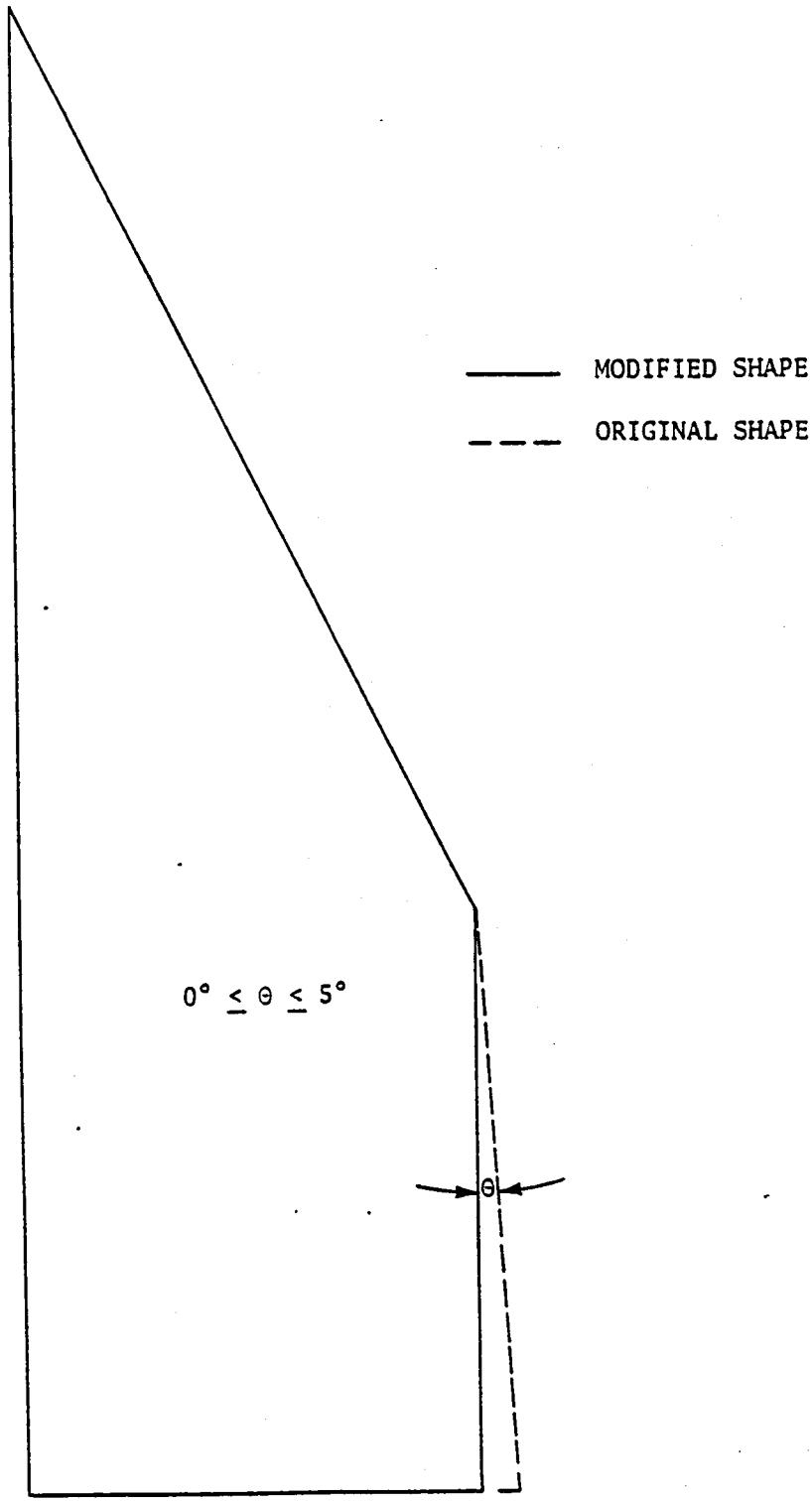

Figure 36. Planforms of modified flat cropped delta wing with different inclinations of the tip edge.

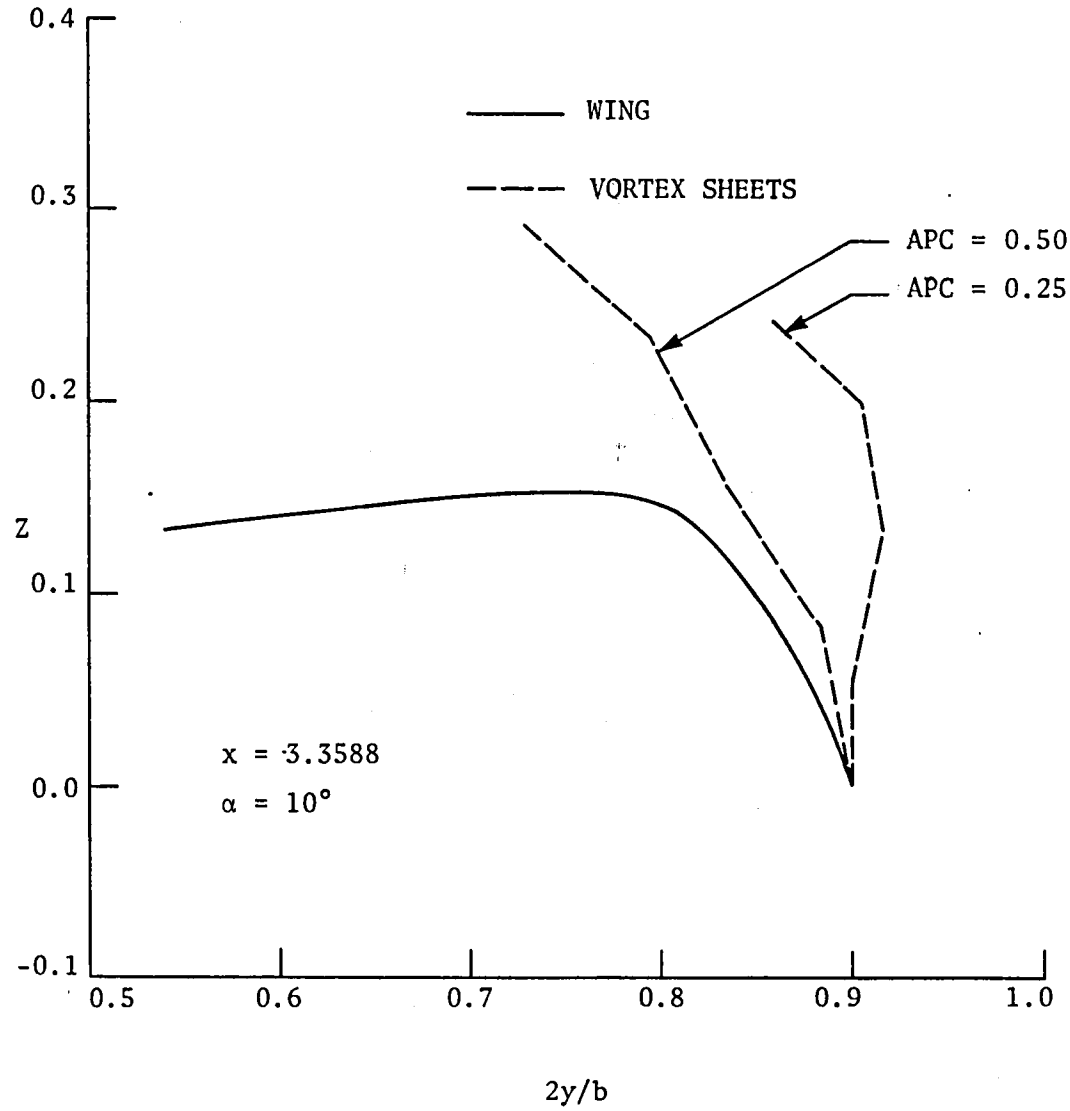

Final 37. Final positions and shapes of vortex sheets with different APC values for A = 1.07 cambered delta wing.

1. Report No.	2. Government Accession No.	3. Recipient's Catalog No.
NASA CR-165706		

4. Title and Subtitle	5. Report Date
Investigation of Aerodynamic Characteristics of Wings Having Vortex Flow Using Different Numerical Codes	April 1981
	6. Performing Organization Code

7. Author(s)	8. Performing Organization Report No.
C. Subba Reddy, Co-Principal Investigator	
	10. Work Unit No.

9. Performing Organization Name and Address	11. Contract or Grant No.
Old Dominion University Research Foundation P.O. Box 6369 Norfolk, Virginia 23508	NSG-1561
	13. Type of Report and Period Covered
12. Sponsoring Agency Name and Address	Contractor Report 9/1/78 - 8/31/79
National Aeronautics and Space Administration Washington, D.C. 20546	14. Sponsoring Agency Code
	505-06-53-01

15. Supplementary Notes

John E. Lamar, Langley Technical Monitor
G. L. Goglia, Co-Principal Investigator, Old Dominion University Research Foundation

16. Abstract

The aerodynamic characteristics of highly sweptback wings having separation-induced vortex flows have been investigated by employing different numerical codes with a view to determining some of the capabilities and limitations of these codes. Flat wings of various configurations—strake wing models, cropped, diamond, arrow and double delta wings, have been studied. Cambered and cranked planforms have also been tested.

The theoretical results predicted by the codes have been compared with the experimental data, wherever possible, and found to agree favorably for most of the configurations investigated. However, large cambered wings could not be successfully modeled by the codes. It appears that the final solution in the free vortex sheet method is affected by the selection of the initial solution. Accumulated span loadings estimated for delta and diamond wings have been found to be unusual in comparison with attached flow results in that the slopes of these load curves near the leading edge do not tend to infinity as they do in the case of attached flow.

17. Key Words (Suggested by Author(s))	18. Distribution Statement
Aerodynamic Characteristics, Accumulated Span Loadings, Free Vortex Sheet, Quasi-Vortex Lattice Method, Suction Analogy Method	Unclassified-Unlimited Subject Category: 02

19. Security Classif. (of this report)	20. Security Classif. (of this page)	21. No. of Pages	22. Price*
Unclassified	Unclassified	57	A04

* For sale by the National Technical Information Service, Springfield, Virginia 22161